55-34

VON KARMAN INSTITUTE FOR FLUID DYNAMICS

LECTURE SERIES 1988-06

PARTICLE IMAGE DISPLACEMENT VELOCIMETRY

MARCH 21 - 25, 1988

SOME COMMENTS ON PARTICLE IMAGE DISPLACEMENT VELOCIMETRY

L.M. Lourenço - The Florida State U., Tallahassee

TABLE OF CONTENTS

1. Introduction

2. Basic Concept

3. Application of Laser Speckle to fluid flow velocity measurement

4. A Guideline for the choice of photographic parameters involved in a measurement using Laser Speckle (LSV) or Particle Image Displacement Velocimetry (PIDV)

5. Accuracy of the Technique

6. Digital Processing

7. Examples of Applications

1. INTRODUCTION

Two of the most important and challenging problems in experimental fluid mechanics are the measurement of the velocity field and the measurement of the vorticity field. Local measurements of the velocity field (i.e., at individual points) are now done routinely in many experiments. However, most of the flow fields of current interest, such as coherent structures in shear flows, are highly unsteady. Hot-wire or laser doppler velocimeter data of such flows are difficult to interpret as both spatial and temporal information of the entire flow field are required and these methods are commonly limited to simultaneous measurements at only a few spatial locations. A quantitative flow visualization technique would be most helpful in the study of these flow fields, providing both the spatial as well as the temporal information. Flow visualization techniques using dye injection or hydrogen bubbles in the case of liquid flows, or smoke injection and smoke wire techniques in the case of air flows have been used to trace streaklines of the injected particles. Despite the fact that valuable information can be derived from the visualization the problem of obtaining an instantaneous velocity map remains. Moreover data obtained from streaklines in unsteady flows must be interpreted with care. Other more sophisticated techniques like streak photography or double exposure techniques of a seeded flow are often used but with limited success (refs 1,2). The reduction of the large amount of information contained in the photograph is far from easy, and the velocity measurements have an associated error which becomes important when the length of the streak, in streak photograph, or the spacing between successive tracer images, in double exposure techniques, is small. Another problem is that these methods fail to provide accurate results when the mean distance between tracers is of the same order of magnitude as the distance a tracer particle travels during the exposure time, in streak photography, or the time between exposures, in double exposure techniques. As a consequence, the tracer concentration is usually kept small resulting in velocity measurements with poor spatial density. Recently rather involved interpolating methods have been designed (ref 3) to increase the spatial resolution of the techniques, but their validity is questionable, considering that in most interesting flows, e.g. separated, turbulent, the distance between existing data points is larger than the flow scales.

Although the vorticity field is an essential property of flows of current interest, mea-

surements of this quantity exceed present experimental capability. This difficulty arises from the fact that vorticity is a quantity defined in terms of local velocity gradients. In contrast, the currently available measurement techniques, such as hot-wire anemometry or laser doppler velocimetry, are sensitive only to the local velocity. Hence, measurements must be made over several points and the resulting velocity components are then analyzed by finite difference schemes. However, the errors produced by the necessary differentiations limit the accuracy and spectral range. In addition, the spatial resolution of this method is often not sufficient to measure small-scale fluid motions or rapidly changing velocity gradients. As a consequence, the measured vorticity field is a type of spatially averaged estimate of the actual vorticity field. Finally, this method provides information at only a single point. If information on the entire flow field is required, measurements must be carried out sequentially one point at a time. This sequential method, although laborious, is straightforward in applications involving steady flows. However, the method becomes very difficult, if not impossible to implement, when studying unsteady flows. Direct measurement of vorticity has been attempted, for example, by injection of spherical particles which rotate in the flow with an angular velocity proportional to the local vorticity (ref 4). Such methods suffer the same drawback of insufficient spatial resolution just mentioned and also can be quite complex.

Recently, a novel velocity measurement technique, commonly referred to as Laser Speckle Velocimetry or Particle Image Displacement Velocimetry has become available. This technique provides the simultaneous visualization of the two-dimensional streamline pattern in unsteady flows as well as the quantification of the velocity field over an entire plane. The advantage of this technique is that the velocity field can be measured over an entire plane of the flow field simultaneously, with accuracy and spatial resolution. From this the instantaneous vorticity field can be easily obtained. This constitutes a great asset for the study of a variety of flows that evolve stochastically in both space and time. This lecture describes the basic concept of Laser Speckle Velocimetry, various methods of data acquisition and reduction, some examples of its use, and some of the parameters that affect its utilization.

2. BASIC CONCEPT

The speckle phenomenon refers to the granular appearance that diffusely reflecting and transmitting surfaces take on when illuminated by coherent light. This grainy appearance is caused by constructive and destructive interference of coherent light (for example, produced by a laser) scattered from a surface element whose roughness is large compared with the wavelength of the laser. For example, when a sheet of paper is placed in the path of laser light, the reflected light contains information on the roughness of the paper. This is the information that is utilized in the Laser speckle context. The first applications of the speckle phenomena were in the field of solid mechanics. It was originally used to measure in-plane displacement and strain of solids with diffusely scattering surfaces and has also been applied to surface roughness measurement, vibration, and deformation analysis. References 5 and 6 review several applications of laser speckle. Typically the basic principle of operation of the Laser speckle technique in solid mechanics applications can be described as follows: A surface is first illuminated by a laser beam, as shown in figure 1. When this surface is imaged through a lens onto a photographic plate, the statistically scattered light gives rise to a speckle pattern. The speckle size is a statistical average of the distance between adjacent regions of maximum and minimum brightness and can be estimated (ref. 5) by the Rayleigh resolution criterion

$$d_s = 1.22\lambda F\#(1 + M) \tag{1}$$

where d_s is the size of a speckle grain, λ is the laser light wavelength, and $F\#$ and M are respectively the F number and magnification of the recording optics. A doubly exposed photograph of the speckle pattern is then recorded, once before and once after a disturbance is introduced. This photograph, or specklegram, contains two correlated grids which can be analyzed as a non-uniform diffraction grating. The technique can only be used when the displacement between exposures is greater than the speckle size, d_s, but not so great as to destroy correlation. Thus, the individual speckle size sets the lower measurable limit.

A convenient method to determine the object displacement uses an underexpanded laser beam to interrogate a small area of the specklegram transparency. The diffraction produced by coherent illumination of the multiple images in the negative generates a Young's

fringes pattern, in the Fourier plane of a lens, provided that the speckle patterns correlate. This is shown schematically in figure 2. These fringes have an orientation which is perpendicular to the direction of the local displacement and a spacing inversely proportional to the displacement. The use of Young's fringes eliminates the difficulties of finding the individual speckle pairs on the photograph. All pairs of the area illuminated automatically combine to yield fringes. However, fringe patterns will appear during the interrogation only if the individual speckle patterns correlate. Displacement of the object other than in-plane translation reduces this correlation and can eliminate the fringe pattern.

3. APPLICATION OF LASER SPECKLE TO FLUID FLOW VELOCITY MEASUREMENT

3.1 Principles

In the application to fluids, the technique involves several steps. First, it is necessary to "create" a selected plane or surface within the flow field. This is accomplished by seeding the flow with small tracer particles, similarly to LDV applications, and illuminating it with a sheet of coherent light, as shown in figure 3. A pulsed laser, such as a Ruby or a NdYag laser, or a CW laser with a shutter, is normally used as the light source. The laser sheet is formed, for example, by focusing the laser beam first with a long focal length lens, to obtain minimum thickness, and then diverging the beam in one dimension with a cylindrical lens. The light scattered by the seeding particles in the illuminated plane provides a moving pattern. When the seeding concentration is low, the pattern consists of resolved diffraction limited images of the particles. When their concentration increases, the images overlap and interface to produce a random speckle pattern. A multiple exposure photograph records this moving pattern.

In a second step the local fluid velocity is derived from the ratio of the measured spacing between the images of the same tracer, or speckle grain, and the time between exposures.

Although the multiple exposed photograph is similar in appearance to one obtained in solid mechanics, there are two fundamental differences. The first is that the fluid is illuminated by a sheet of laser light whose thickness is Δz. Therefore, scattering occurs from a volume distribution of particles rather than a surface distribution. Secondly, the number density of particles per unit volume can vary over a wide range of values, depending upon the fluid studied and the seeding concentration. As previously mentioned for a true speckle pattern to exist, the number of scattering particles must be quite high so that the particle images overlap and interface in the image plane. When the particle concentration is lower than this level, discrete images of the particles will be photographed. This low particle concentration originates a mode of operation of the technique referred as Particle Image Displacement Velocimetry, reserving the term Laser Speckle Velocimetry for the high particle concentration levels where a random speckle pattern is actually formed.

3.2 Retrieval of Flow Field data

Several methods exist to convert the information as the multiple-exposed photograph, or specklegram, to flow field data such as velocity or vorticity. The recorded image, whether formed by isolated disks, in the case of low particle concentration, or speckle grains for high particle concentration is a complicated random pattern. It would be very difficult to measure the local displacements by visual or computer-aided inspection. However, it is important to realize that the multiple exposure photograph results in a periodic random image from which the periodicity information can be retrieved using Fourier analysis. Basically, the multiple-exposed photographs or specklegrams can be analyzed either on a point-by-point basis, which yields measurements of the local displacements (velocity), or with a whole field filtering technique, which yields isovelocity contours. Recently a third method has been proposed by Collicott and Hesselink, (ref. 7). This method consists of an anamorphic optical system which forms a 1-D Fourier transform in the x-direction for measuring the x-velocity component, and images the speckle pattern in the y-direction. This results in curved fringes which have a local spacing inversely proportional to the x-velocity at that point. Simultaneous multiple point measurements are obtained by imaging in the y-direction. Thus it is possible to measure a velocity component along a selected line in the flow.

In this lecture only the first two methods are presented. A brief discussion on alternative fully digital method of analysis will also be included.

3.2.1 Local Velocity measurement using the Young's fringe method

Consider the function $D(\vec{r})$ describing the light intensity in the image plane of a photographic camera, where $\vec{r}(x,y)$ are the plane coordinates. Considering that there is an in-the-plane displacement dy of the scatterers, the image will be translated by Mdy, where M is the magnification of the camera lens, and the intensity distributions is

$$D(x,y) + D(x,y + Mdy) = D(x,y) \oplus \left[\delta(x,y) + \delta(x,y + Mdy)\right] \qquad (2)$$

where $\delta(x,y)$ is the Dirac delta function centered on $\vec{r}(x,y)$, and considering that a translation can be represented as a convolution with a delta function. The total intensity

is recorded on photographic plate. After development the transmittance, τ, of the negative is given

$$\tau(\vec{r}) = a + bD(x,y) \oplus \left[\delta(x,y) + \delta(x,y+Mdy)\right] \tag{3}$$

where a and b are characteristic constants of the photographic emulsion. Local analysis of the film negative with a probe laser beam (fig. 2) produces in the focal plane of a lens a two dimensional Fourier transform of the transmittance distribution, $\tilde{\tau}$, as follows:

$$\tilde{\tau}(u,v) = a\delta(u,v) + b\tilde{D}(u,v)\left[1 + \exp\left(\frac{i2\pi vMdy}{\lambda_a}\right)\right] \tag{4}$$

where $\tilde{\tau}$ represents the Fourier transform of τ, u and v are the angular coordinates of a point in the Fourier plane of the lens, and λ_a is the wavelength of the interrogating laser light beam.

The first term, $a\delta(u,v)$ on the r.h.s. of equation (4) represents the image of a point source, i.e. the interrogating beam, when diffraction effects are neglected. This image is seen as a small bright spot in the center of the Fourier plane. The second term is composed by a fine speckle structure, $\tilde{D}$ (diffraction halo) modulated by

$$\left\{1 + \exp\left(\frac{i2\pi vMdy}{\lambda_a}\right)\right\} \tag{5}$$

The intensity distribution for the second term is obtained by multiplication with its complex conjugate, resulting in

$$|\tilde{D}(u,v)|^2\left[4\cos^2\frac{\pi vMdy}{\lambda_a}\right] \tag{6}$$

The diffuse background, $|\tilde{D}|^2$, (called "diffraction halo" is modulated by a set of Young's fringes whose spacing is given by

$$d_F = \frac{\lambda_a f_L}{Mdy} \tag{7}$$

where f_L is the focal length of the converging lens. Knowing M, f_L, λ_a and measuring d_F the displacement dy is easily found from equation (7), with the direction of motion perpendicular to the orientation of the fringes. A typical example of a Young's fringes pattern is shown in the photograph of figure 4.

By scanning the double exposed photograph one can resolve the two components of the velocity vector at every point of the field. This is a unique feature of the laser speckle technique.

3.2.2 Velocity measurement by spatial filtering

Processing the photograph with a conventional spatial filter (Fig. 4) provides directly a velocity map of the two dimensional flow pattern. This method is fast and convenient. The transmittance of the photograph is given by

$$\tau(\vec{r}) = a + b\left[D(\vec{r}) \oplus \sum_{k=0}^{N-1} \lambda(\vec{r} + kM\ \vec{d})\right] \tag{8}$$

where $\vec{r}$ is the position vector, $\vec{d}$ the displacement and N the number of exposures.

In the Fourier plane, the amplitude is expressed in the form:

$$U(\vec{r_f}) = TF\Big(T(\vec{r})\Big)P(\vec{r_f}) \tag{9}$$

where $\vec{r_f}$ is the position vector in the Fourier plane, TF means a two dimensional Fourier transform and $P(\vec{r_f})$ is the transmittance of the filter.

If the filter is a circular hole (with radius a), whose center is located at $\vec{r_0}$, corresponding to a spatial frequency $\vec{r} = \vec{r_0}/\lambda_f$, the intensity in the image plane may be expressed by

$$I(\vec{r_p}) = C\left|\tau(-\vec{r_p}) \oplus \left(\exp(-2\pi j\ \vec{r_p}\ \vec{f_0}\right) \frac{J_1\left(\frac{2\pi r_p a}{\lambda_f}\right)}{\left(\frac{2\pi r_p a}{\lambda_f}\right)}\right|^2 \tag{10}$$

where $\vec{r_p}$ is the position vector in the image plane, C is a constant, λ_f is the wavelength and f is the focal length of the transform lenses.

The convolution in equation (10) will be extreme in the regions where the projection Md_p of the displacement on the direction defined by the filtering hole is a multiple of the period of the oscillatory term $\exp(-2\pi j\ \vec{r_p}\ \vec{f_0}$. The projected displacement d_p obeys the relation $Md_p = \frac{n\lambda}{\Theta}$, where n is an integer and Θ the angle shown in figure 5. Thus isovelocity contours are drawn by the spatial filter. The interferences between independent particles contained in the area defined by the factor $J_1(\frac{2\pi r_p a}{\lambda f})/(\frac{2\pi r_p a}{\lambda f})$ in equation (10) produce the speckle present in the filtered image. It must be pointed out that the quality of the isovelocity fringes is essentially a result of the multiple exposure technique. The

multiple beam interference causes the same sharpening and increase in brightness of the isovelocity fringes as in a Fabry-Perót interferometer.

The whole-field measurement by spatial filtering, although very appealing because it quickly gives isovelocity contours, has several drawbacks. First, the filtered images of an unknown flow field can be difficult to interpret, so several images of the same specklegram with different filters may be required to understand the flow. Thus, it may be limited to the study of rather simple flows, or flows about which much is already known. A second problem concerns the filtering technique itself. This process reduces the resolution and necessitates strong illumination to avoid intensity problems. The use of the local velocity measurement technique described above are believed better for quantitative information.

4. A GUIDELINE FOR THE CHOICE OF THE PHOTOGRAPHIC PARAMETERS INVOLVED IN A MEASUREMENT USING LASER SPECKLE (LSV) OR PARTICLE IMAGE DISPLACEMENT VELOCIMETRY (PIDV)

This section describes some of the parameters that can affect the use of either laser speckle velocimetry or particle image displacement velocimetry. The impact of these parameters is discussed and, where possible, recommended values are given.

The technique relies on the ability to detect and record on a photographic plate the images of the seeding particles. This image is a function of the scattering power and concentration of the particles within the fluid, the amount of light in the illuminating sheet, magnification of the recording optics, and film sensitivity at the wavelength of the illumination laser light.

The specific parameters playing a role in either Laser Speckle Velocimetry or Particle Image Displacement Velocimetry include the following:

1) Tracer (type, dimension, and concentration)

2) Exposure parameters (duration of exposure, time between exposures, and number of exposures)

3) Film parameters (sensitivity, grain size, and resolution)

4) Recording Optics (magnification, lens aperture)

4.1 Tracer

Tracers to be used in a measurement involving LSV or PIDV have to be as small as possible to accurately follow the fluid motions, and good light scatterers. These requirements are usually met by tracers used in LDV applications. In liquid flows we recommend the use of pliolite particles, which are practically neutrally buoyant in water, latex and titanium dioxide. In air flows, oil smoke or fog produces a relatively uniform seeding.

As previously mentioned, the light scattered by the seeding particles can create, depending on the seeding concentration, two entirely different patterns. This originates two modes of operation of the technique. For low seeding concentrations, the pattern consists of resolved diffraction limited images of the particles. When this concentration increases,

the images overlap and interfere in the image plane to produce a random speckle pattern. In either case, the pattern is recorded in a multiple exposed photograph, from which the velocity data is obtained. However, in the Particle Image mode of operation, due to light seeding, regions of the flow field may be left unseeded, or with poor seeding, resulting in signal drop-out. On the other hand, in the Laser Speckle mode of operation, the drop-out problem is minimized, but other more restrictive complications may occur, as described below. These problems preclude the use of the Laser Speckle mode of operation in the majority of flow fields of interest.

The Laser Speckle mode of operation relies on the recording of identical laterally shifted speckle patterns. Slight out-of-plane motion of the scatterers, due to flow three-dimensionality, between the exposures results in speckle patterns that are not entirely similar. As a illumination does not produce Young's fringes, or produces fringes with poor contrast and signal to noise ratio (SNR). This poses a severe limitation in the use of the Laser Speckle Displacements for the measurement of velocity in turbulent flows, or flows with an important velocity component in the direction perpendicular to the measuring plane. The fringe quality becomes less dependent on the out-of-plane motion when individual particle images are imaged and recorded, i.e. in the Particle Image mode of operation. In this case the tolerance to out-of-plane motion is roughly equivalent to the width of the illumination sheet and focusing depth of field of the recording optics. In addition, the high concentrations required by the Speckle mode of operation cause multiple scattering effects which result in the spreading of the thin laser illuminating sheet. Furthermore, the high concentration of tracers may strongly influence the flow field.

In conclusion, for a successful measurement using this technique, there are practical bounds to seeding concentration. The upper boundary for the seeding concentration being set by a value above which a speckle pattern is formed due to the interference of light scattered by the individual particles. If Cp is the particle concentration and ΔZ the width of the laser sheet, we obtain for the maximum concentration

$$\sqrt{\frac{1}{\Delta Z Cp}} >> \frac{d_1}{M} \tag{11}$$

where d_i is the particle image diameter. Considering typical values for $dp = 0.03mm$ and

$\Delta Z = 0.5mm$ and $M = 1$ we obtain $Cp << 2.10^{12}m^{-3}$.

The lower end for the seeding concentration can be determined by considering that, in order to have a valid measurement, a minimum number of particle image pairs must be present in the area scanned by interrogation beam. The case of having a single particle image pair in the interrogation area is an ideal one, because it yields fringes with optimum SNR. However, this situation can only be achieved by lightly seeding the flow, thus giving rise to the so-called drop-out problem. An interesting case occurs when only two particle pairs are present in the interrogation area. The corresponding diffraction pattern includes multiple equally intense fringe patterns due to cross interference of non-corresponding image pairs. In this case, the local displacement cannot be resolved (Fig. 6). Finally, as the number of particle image pairs in the interrogation area increases, the cross interference fringes become weaker in comparison with the "main fringe pattern" which reflects the local displacement (Fig. 4). The cross-interference fringes are sometimes designated as a "background speckle noise." Our experience shows that, for reasonable fringe quality, at least four particle image pairs need to be present in the interrogation area. This number can be somewhat relaxed if more than two exposures were used for the photography. Considering that these particles exist in the volume defined dy the width, ΔZ, of the laser sheet, scanned by the beam whose diameter is D, e.g. $D = 0.5mm$, we obtain for the average concentration:

$$Cp = \frac{16}{\Delta Z \pi D^2} \simeq 10^{-11} m^{-3} \tag{12}$$

4.2 Exposure Parameters

The exposure parameters are chosen in accordance with the maximum expected velocity in the field and the required spatial resolution. The spatial resolution, which is equal to the cross sectional area of the interrogating laser beam, is dictated by the scales involved in the fluid motion and should be less than the smallest scale.

The time between exposures, T, is determined by the maximum permissible displacement of a particle such that a correlation is obtained when locally analyzing the film negative with the probe laser beam. A necessary condition to obtain Young's fringes requires that the distance between adjacent particle images be less than a fraction of the analyzing beam diameter. In practice the maximum permissible displacement that can be

detected corresponds to the case when the fringe spacing, d_F, is larger than the diffraction limited spot size, d_s, of the interrogating optics. In analytical terms:

$$d_f = \frac{\lambda_a f_L}{M v_{max} T} > d_s = \frac{4\lambda_a F_L}{\pi D} \tag{13}$$

where M is the magnification factor, D and λ_a are respectively the interrogation beam diameter and laser light wave-length. We obtain for the time between exposures

$$T = \frac{0.5D}{M v_{max}} = \frac{1}{F} \tag{14}$$

v_{max} is the maximum expected velocity in the field, and F the frequency corresponding to the inverse of the period T. For practical purposes we use the constant 0.5 instead of 0.8 as it would be given by equation 13.

The exposure time, t, is a free parameter when a CW laser source is used together with a shutter. In previous applications (ref. 8-10) the exposure time has been kept as small as possible for minimum particle image size. In a later study, Lourenco (ref 11) demonstrated that the duration of the exposure time can be of the same order of magnitude as the time between exposures.

For very short exposures the recorded particle images are identical to the diffraction limited particle images as the particles appear to be stationary during the exposure. For longer exposures the recorded images become streaks whose length is directly proportional to the exposure time. Coherent illumination of these images generates Young's fringes superposed on a diffraction pattern which depends on the streak length. In the limiting case of a very short exposure, the diffraction pattern is symmetric and has a circular shape. When the exposure time is increased, small streaks are generated, and the diffracted light in the spectrum is concentrated in a band whose width is inversely proportional to the streak length.

Because of the finite width of the diffraction pattern, the number of fringes, n_F, in the pattern becomes a function of the ratio between the streak separation to the streak length, l_s. In analytical terms:

$$n_F = \frac{dy}{l_s} + 1 \tag{15}$$

For an accurate measurement of the fringe spacing, it is necessary to have a reasonable number of bright fringes. Usually five bright fringes give good results.

Another parameter determining the degree of accuracy with which the fringe spacing can be determined is the contrast and sharpness of the Young's fringes. If the number of exposures, N, is larger than two and the particles are displaced by the same amount after each exposure, the sharpness of the interference fringes can be greatly improved.

For a multiple exposure, the function describing the light intensity of the point sources becomes

$$D(x,y) \oplus \sum_{n=0}^{N-1} (x, y + nMdy) \tag{16}$$

resulting in an amplitude distribution of the transmittance of the negative in the Fourier plane of a lens, as follows:

$$|\tilde{D}(u,v)|^2 \left\{ N + 2 \sum_{n=1}^{N-1} n \cos \left[(N-n) 2\pi M \frac{dy}{\lambda_a} \right] \right\} \tag{17}$$

For a number of exposures, N, equal to two a relation similar to equation 4 is obtained as expected.

Figure 7 displays the fringe width for multiple exposures, normalized with the corresponding width for a double exposure, versus the number of exposures. It is clearly seen that an optimum fringe width can be obtained with a limited number of exposures.

The sharpening of the fringes using a multiple exposure recording technique is of great advantage because it allows a very easy visual and qualitative "measurement" of the direction and spacing of the Young's fringes. It also increases their signal to noise ratio. Note that this improvement in the signal to noise ratio is a result of the artificial increase in particle concentration due to the multiple exposure.

4.3 Choice of the Film and Laser Power Requirements

The technique relies on the ability to detect and record on photographic media the seeding particles images. The particle is a function of the scattering power of the particles within the fluid, the amount of light in the illuminating sheet, camera lens and film sensitivity at the wavelength of the illuminating laser light. Although the particle detection increases proportionally with increasing power of the illuminating laser, it is of great importance to keep the laser power requirement to its minimum. An important reason for

this limitation is economy as the main component in the cost of the apparatus is the laser source and its price increases very rapidly with the power delivered.

In this section, we suggest films to be used and the laser power required to expose these films.

To compensate for the limited illuminating laser power, the films used to record the particle images, are required to have good sensitivity, but without sacrificing film resolution. When good precision is necessary, films with a resolution of about 300 line-pairs/mm and sensitivity from 25 to 125 ASA (Afga Ortho 25, Kodak Technical Pan 2415) are suitable for the use either with pulsed Ruby lasers ($\lambda \simeq 700nm$) or pulsed, frequency doubled, NdYag lasers and CW Argon-Ion lasers ($\lambda \simeq 500nm$). When a NdYag or a CW Argon-Ion laser are used, such as Kodak TMAX 400ASA and the Kodak Royal-X Pan, 1250 ASA, which have excellent sensitivity in 400-600nm range, and retain fairly good resolution (100 line-pairs/mm).

Another parameter to be accounted for is the film grain. When illuminating the film negative to produce Young's fringes, the film's unexposed grains can introduce amplitude and/or phase changes into the wavefront of the analyzing laser beam and thus create additional noise. This noise has generally a frequency content which is in the same range as the Young's fringes. Therefore its elimination is difficult either from optical or digital filtering. Film grain cannot be totally eliminated and it will always be present in different degrees, especially in applications where fast film is used, to cope with low power density of the illuminating sheet. A method of solution as been proposed (ref 12) by which this source of noise is considerably reduced. It consists of producing a positive copy by contact printing on a very high resolution fine grain film, for example holographic plates. The positive copy is analyzed in the same manner using the laser probe beam. With this method, a remarkable decrease in noise level is achieved. Another advantage of using this procedure is that the intensity of central zero order spot, due to the laser probe beam, is also decreased or eliminated.

Once the film is selected, the amount of laser power required for the exposure can be computed. For a successful exposure of the photographic emulsion the energy scattered by a tracer particle and viewed through the camera lens has to be larger than the film sensitivity

at the wavelength of the illuminating laser. It is customary to write this condition in the following analytical form:

$$\overline{E} = \int_{\Delta t} \Upsilon dt > CE_o \tag{18}$$

where $\overline{E}$ is the mean exposure level for a single particle (J/m^2), Υ is the average intensity of the light scattered by a particle (W/m^2), E_0 is the film fog level and Δt is the exposure time. C is a constant between 1 and 10. The fog level is defined as the exposure level below which the transmissivity of the film is independent of the incident intensity (Fig. 8). The average intensity, Υ, of the light scattered by a single particle can be expressed in terms of (ref. 13)

$$\Upsilon = \frac{4}{\pi k^2 d_1^2} I_o \int_\Omega \sigma^2 d\Omega \tag{19}$$

where I_o is the intensity of the illuminating sheet ($\frac{W}{m^2}$), k is the illuminating laser light wavenumber, $\sigma = \underline{\sigma} \cdot \underline{\sigma}^*$ is the Mie parameter, Ω the viewangle of the camera lens and d_i is the dimension of the diffraction limited particle image composed of two terms (10), neglecting aberrations and grain noise, as follows:

$$d_i = \sqrt{d_p^2 + d_e^2} \tag{20}$$

The first one being the particle diameter and the second one the edge spread caused by the limited response of the recording optics

$$d_e = 2.44\lambda(1 + M)F\# \tag{21}$$

with $F\#$ the camera objective F number.

When a pulsed laser is used the laser power required is simply determined from equation 19, considering that the particle is stationary during the exposure

$$I_o > \frac{CE_o(\pi K^2 d_p^2)\Delta t}{4 \int \sigma^2 d\Omega} \tag{22}$$

Considering that for a pulsed laser the pulse duration (= exposure time) is a fixed parameter, it is customary to express equation 22 in terms of energy per pulse, ϵ_o

$$\epsilon_o > \frac{CE_o(\pi K^2 d_p^2)}{4 \int \sigma^2 d\Omega} \tag{23}$$

The recommended value for the constant C is between 3 and 5 to compensate for film reciprocity effects caused by the very short exposure.

In applications involving the use of CW laser the exposure time is variable and considerably longer. In this case integration of equation 18 is somewhat more elaborate. For the sake of simplicity let us assume that the fluid motion, and hence the seeding particles displacement is unidimensional. Let r_o, r and u be respectively the initial position, current position and velocity of a tracer particle, in the film plane. The current particle position can be expressed as

$$r = r_o + ut \tag{24}$$

The exposure can be determined integrating equation 14 and considering two cases, $t < \frac{d_i}{u}$ and $t \geq \frac{d_i}{u}$

$$\overline{E} = \int_{\Delta t < \frac{d}{-i}_u} \Upsilon(r)dt = \begin{cases} \Upsilon\frac{(r-r_o)}{u} & r_o < r \leq r_o + u \cdot \Delta t \\ \Upsilon\Delta t & r_o + ut < r < -r_o + d_i \\ \frac{\Upsilon}{u}(r_o - r + d_i + u\Delta t) & r_o + d_i < r \leq r_o + d_i + u \cdot \Delta t \end{cases} \tag{25}$$

$$\overline{E} = \int_{\Delta t > \frac{d}{-i}_u} \Upsilon(r)dt = \begin{cases} \Upsilon\frac{r-r_o}{u} & r_o < r \leq r_o + d_i \\ \Upsilon\frac{d}{-i}_u & r_o + d < r \leq r_o + d_i u \cdot \Delta t \\ \frac{\Upsilon}{u}(r_o - r + 2d_i + u\Delta t) & r_o + d + u \cdot t < r \leq r_o + 2d_i + u \cdot \Delta t \end{cases}$$

The maximum exposure is obtained for exposure times larger or equal to $\frac{di}{u}$. Thus, for the whole field, the optimum exposure, is equal to $\frac{d_i}{V_{max}}$ which results in the maximum exposure, without a significant reduction on the dynamic range of the technique, as shown in the following section.

The CW laser power required is given by,

$$I_o \geq \frac{CE_o(\pi K^2 d_1^2)V_{max}}{4\int \sigma^2 d\Omega d_i} \tag{26}$$

Equation 26 shows that CW laser power required for a measurement increases with the flow velocity. This limitation does not apply to the case of a pulsed laser where the pulse duration is independent of the flow velocity.

4.4 Velocity Dynamic Range

In the following we will analyze the technique's abilities of resolving large velocity gradients in flow fields, i.e. its dynamic range. The dynamic range is defined as the largest velocity difference that can be detected in the flow field.

The low end of the dynamic range is determined by considering that for a measurement the spacing between the successive particle diffraction limited images or streaks is well resolved, i.e. do not collapse on each other. In analytical form

$$l_s = d_i + V \cdot t < V \cdot T \tag{27}$$

Considering that the time between exposures, T, is a function of the maximum velocity V_{max}, substituting $t \simeq o$ for a pulsed laser and, $t = \frac{d_i}{V_{max}}$ for a CW laser, yields the following expressions for the minimum velocity,

$$V_{min} = \frac{2MV_{max}d_i}{D} \qquad \text{pulsed laser} \tag{28}$$

$$V_{min} = \frac{2MV_{max}d_i}{D_2 M d_i} \qquad \text{CW laser} \tag{29}$$

The velocity difference $V_{min} = \frac{V_{Max} - V_{min}}{V_{min}}$ is the velocity dynamic range and we obtain,

$$\Delta V = \frac{D}{2M d_i} - 1 \qquad \text{pulsed laser} \tag{30}$$

$$\Delta V = \frac{D - 2d_i}{2M d_i} - 1 \qquad \text{CW laser} \tag{31}$$

The dynamic range increases with shorter pulse durations and is maximum in applications involving the use of a pulsed laser. Considering typical values for $di = .03mm$, $D = 0.5mm$ and $M = 1$, we obtain for the dynamic range,

$$\Delta V \simeq 7.5 \quad \text{pulsed laser} \tag{32}$$

$$\Delta V \simeq 6.5 \quad \text{CW laser} \tag{33}$$

5. ACCURACY OF THE TECHNIQUE

The overall accuracy of the technique depends on the accuracies which can be achieved in the photographic procedure and processing techniques.

5.1 Photographic Procedure

Let us first consider the photographic procedure. The sources of error are the lens aberrations and the limited film resolution, causing the position of the particles to be recorded with an inherent error, and the spurious contributions on the in-plane displacement recording by the out-of-plane motion.

In section 4.1 it was pointed out that out-of-plane motion was a severe limitation on the use of speckle in Fluid Dynamics applications. The reason for this limitation was that slight out-of-plane motion by the scatterers, between the multiple exposure, results in non-identical shifted patterns poorly correlated. To cope with this problem one operates in the Particle Imaging mode, where the particles are directly imaged and recorded. However, as shown in the following, out-of-plane motion may also contribute to considerable errors in the velocity measurement.

Let us consider the imaging system of figure 9 and the particle in position P_o within the laser sheet. Between exposures the particle moves to a position M_o, due to three-dimensional fluid motion. The components of the displacement vector are dx, dy, dz, with dx and dy, the in-plane and dz the out-of-plane components of the displacement. In the image plane the photographic plate records the position of the particle at P_L and M_L. The coordinates of these points are given by:

$$\left.\begin{matrix} -Mx \\ -My \\ d_o + d_L \end{matrix}\right\} P_L \qquad \left.\begin{matrix} -M(x+dx)(1+dz/dL) \\ -M(y+dy)(1+dz/dL) \\ d_o + d_L \end{matrix}\right\} M_L \tag{34}$$

where second order terms have been neglected for simplicity.

The displacement $P_L M_L$, measured by means of Young's fringes is given by

$$dx_m = Mdx\left(1 + \frac{xdz}{dxd_L}\right) \qquad dy_m = Mdy\left(1 + \frac{ydz}{dyd_L}\right) \tag{35}$$

and the measured displacement components referred to the object plane are

$$dx_o = dx + \frac{xdz}{d_L} \qquad dy_o = dy + \frac{ydz}{d_L} \tag{36}$$

The contribution of the out-of-plane displacement to the measured displacement is given by two parasite terms $(\frac{xdz}{d_L})$ and $(\frac{ydz}{d_L})$. The error produced by the out-of-plane motion while negligible in the neighborhood of the optical axis, increases linearly, and may become important, with the distance from the optical axis. The influence of the out-of-plane motion becomes particularly important when imaging the flow with short focal and wide angle objectives.

A relation can easily be found for the theoretical error in a measurement due to out-of-plane motion:

$$E_x = \frac{dx}{dx} \tan \psi_x \qquad (37)$$
$$E_y = \tan \psi_y$$

where ψ_x and ψ_y are respectively semi-field angle components along the x and y axis respectively. Hence the error depends only on the ratio of the out-of-plane to in-plane component of displacement and the tangent of the semi-field angle.

5.2 Correction for out-of-plane motion

Analysis of figure 9 shows that in applications were large fields of view are involved (large magnifications and short focal length) and there are considerable out-of-plane motions, the errors in the measurement of the in-plane components may become important. This fact stresses the necessity for the implementation of techniques aiming at the elimination of the out-of-plane influence in the measurement. Here we present a technique which has been developed in the metrology of body displacements using white light speckle photography by Jacquot and Rastogi (ref. 14). This technique although developed specifically for white light speckle photography, can be generally applied to coherent speckle photography or particle multiple exposure techniques, since the motion of speckle grains or particles are governed by the same geometrical laws.

The principle of the method consists of imaging a point, P_0, in the illumination sheet in two distinct directions as shown in figure 10 and the point P_0. Its positions can be restored from its two images P_1 and P_2 by tracing back the two lines P_1L_1 and P_2L_2 to their intersection. The individual displacement P_1L_1 and P_2L_2 can be measured by the Young's fringe analysis method and provided that the direction of the displacement is known, the intersection of the lines M_{1L} and M_2L_2 gives the point $M_0(x + dx, y + dy, dz)$. Therefore,

using this method it is possible to retrieve the three components of the displacement.

A practical optical setup presented in reference 14 uses two viewing objectives arranged parallel and decentred with respect to the optical axis. This method is denominated 'Lateral decentring method'. The objectives are decentered respectively by $(\delta x, \delta y)$ for L_1 and $(-\delta x, -\delta y)$ for L_2. The relations governing the measured displacement components become:

$$\begin{aligned} dx_{1_m} &= dx + \frac{dz}{d_0}(x + \delta x) \\ dy_{1_m} &= dy + \frac{dz}{d_0}(y + \delta y) \\ dx_{2_m} &= dx + \frac{d_z}{d_0}(x - \delta x) \\ dy_{2_m} &= dy + \frac{d_z}{d_0}(y - \delta y) \end{aligned} \tag{38}$$

which yields, for the displacement components,

$$\begin{aligned} dx &= \frac{x(dx_{2_m} - dx_{1_m}) + \delta x(dx_{2_m} + dx_{1_m})}{2\delta x} \\ dy &= \frac{y(dy_{2_m} - dy_{1_m}) + \delta y(dy_{2_m} + dy_{1_m})}{2\delta y} \\ dz &= \frac{d_0}{2\delta x}(dx_{1_m} = dx_{2_m}) \end{aligned} \tag{39}$$

The displacement components can therefore be determined according to equations and using the values of dx_m and dy_m previously measured by the Young's fringe method.

The limitations of this method are that the maximum out-of-plane motion which is permissible is less than the illumination sheet width.

Accuracy considerations also show other method limitations. Neglecting measurement errors in the evaluation of δx and δy (decentring parameters), an error analysis yields for the errors in the computed displacement:

$$\begin{aligned} \frac{\Delta(dx)}{dx} &\cong \frac{\Delta(dx)_m}{dx_m} 1 + \frac{x}{\delta x} \\ \frac{\Delta(dz)}{dz} &\cong \frac{\Delta(dx)_m}{dx_m}\left(\frac{x}{\epsilon_x \delta x}\right) \end{aligned} \tag{40}$$

Equations 40 show that the errors are minimized for small $\frac{x}{\delta x}$. There is a practical limit in the upper value of δx which is set by the aberrations of the lens.

The above described technique is just an example of a method of solution to remedy the influence of out-of-plane motion. For each individual application different optical setups may be designed, having different performances. Nevertheless, it is important to keep in mind that these methods do not provide compensation for out-of-plane motion which is larger than the illumination sheet thickness.

5.3 Accuracy of the processing techniques

The accuracy of the methods described in section 3 can be evaluated in a simple way. Because it is extremely difficult to produce experimentally a fluid flow whose characteristics are known with an accuracy better than 1it was necessary to perform measurements in an artificial uniform velocity field. A suspension of particles ($4\mu m$ diameter) in water is photographed with magnification 0.5. A uniform displacement field is obtained by producing a multiple exposed photograph of the still seeded fluid with a camera moving at constant speed. A large number of points of this photograph are analyzed by means of the above techniques in order to obtain statistical information about the experimental errors.

It is important to note that the measurement errors are due to the speckle present in the fringes. Since this speckle is the result of the random distribution of independent particles located in the illuminated region, the velocity evaluation must be viewed as the measure of a random variable. In the absence of systematic bias (sufficiently large fringe density), the standard deviation of the distribution is an estimate of the mean measurement error. When analysis is performed using a $0.5mm$ diameter beam, the maximum measurable displacement is $\tilde{2}00\mu m$. Beyond this value the contrast of the fringes decreases strongly. For a $200\mu m$ displacement, a sequence of sixty measurements is performed at different points of the photography. Analysis by the two techniques yields the same mean value ($0.25\mu m$ mean difference) with a nearly equal standard deviation of $2.5\mu m$ (1.25% of the maximum displacement). The same values are obtained for a displacement of $150\mu m$. This mean error can be significantly larger than the inaccuracy quoted in solid mechanics (relative error $< 1\%$). This can be explained by the fact that, due to the absence of a classical speckle on the photograph, the shape of the diffraction halo can be distorted and so contributes to the measurement error. On the other hand, the optical Fourier transform performs a two dimensional correlation between two successive images of the same par-

6. DIGITAL PROCESSING

The digital image analysis system Fluid Mechanics Research Laboratory of The Florida State University is presented in figure 11. The Fringe images are acquired and digitized via a black and white analog camera, by the Digital Video Processor and the frame digitizer. The Digital Video Processor provides the synchronization signals and its capability of digitizing up to 30 frames per second. The digitized video signal is on one of four memory board. This board has 512 x 512 pixel resolution and each 8 bit per pixel, allowing up to 256 gray or false color scales. The imaging system has built-in a high speed 8 bit video D/A converter and for each color and graphics channel a bank of 4 gray scale/color encoders channel.

These encoders supply a video black/white or color output which is displayed on a video monitor. This system is computer controlled (Micro VAX II) through a Q-Bus interface. Transfer between the IP8500 memories and the Micro VAX II memory disks or magnetic tape is also possible.

The fringe processing system is also shown in figure 11. The camera C is focused on the plane F where the Fourier transform of the illuminated region (typically $0.5mm$ in diameter) is located. The fringe images are then digitized in a 512x512 format. In the following sections, two complementary methods for fringe analysis are presented.

6.1 Processing of Young's fringes data

Let us assume that the fringe intensity $F(u,v)$ is digitized and stored in a square matrix of the form $I(m,n)$. Furthermore, it is assumed that the digitization process satisfies the Shannon criterion with $0 > m,n > 511$. The most popular processing algorithms fall in the following categories:

Interactive methods and fully automated methods

6.1.1. One-dimensional-averaging technique

Interactive processing of the fringes can be performed easily by a simple method currently used in solid mechanics. The principle is to obtain a periodic signal by averaging over the lines (or the columns) of the picture. However, it is necessary to measure in-

ticles. However, given the limited resolution of the film, these images are not absolutely identical. Because of the low intensity of light that impinges on the film, the latter must be of high sensitivity (Kodak 2415 instead of holographic plates). That images of the particles cannot be compared with a precision higher than $2.5\mu m$ may be due to the limited resolving power over such a film (320 lines/mm).

dependently the angle of the fringes, which is performed by superimposing a computer-generated line on the digitized picture and adjusting its direction until it is parallel to the fringes. Considering that the fringes are totalted of an angle α to become parallell to the n-axis we obtain:

$$I(m,n) = S(m)H(m,n) \tag{41}$$

where $S(m)$ is the periodic term with a contrast not necessarily equal to one, and $H(m,n)$ a signal component due to the diffraction halo.

Integrating over the n-axis results in:

$$f(m) - S(m) \sum_{n=0}^{N-1} H(m,n)$$

or (42)

$$f(m) = S(m)Ho(m)$$

where $Ho(m)$ is a function representing the averaged fringe intensity envelope. Being $I(m,n)$ the digitized intensity, α the angle of the fringes along the n-axis and if (255, 255) are the coordinates of the center of the picture, the previous operations can be implemented using the formula:

$$f(m) = \sum_{n=0}^{511} I[m + (n - 255)\tan\alpha, n] 0 \leq m \leq 511 \tag{43}$$

is proportional to the velocity component along the m axis. Note that this procedure eliminates the need for mechanical rotation of the fringes. Further, Fourier processing of $f(m)$ yields the value of its periodicity. However, it can be shown that $f(m)$ is the product of an envelope waveform which results from the diffraction halo (see equation 4 and 6). The Fourier transform of $f(m)$ is the convolution of a Dirac distribution with the transform of the envelope which can be a broad function with important side lobes. To minimize the linewidth, a constant amplitude periodic function must be recovered from $f(m)$. In solid mechanics, the envelope can be evaluated by integrating the fringe intensity along a direction perpendicular to the fringes. Because of the difficulty of measuring, this envelope in fluid mechanics applications, due to the large speckle grain in the fringes, the minimization procedure can be performed by computing the logarithm of $f(m)$ or its

derivative. The logarithmic transformation is based on the cepstrum technique used in acoustics and transforms the product constituting $f(m)$ into the sum of a nearly constant amplitude function and a slowly varying waveform. As a result, the power spectrum of $\log f(m)$ will show a narrow peak at the fringe frequency. The derivative of $f(m)$, $f\prime(m)$ is a high pass filtered version of the original signal and therefore the slowly varying envelope component is eliminated. Again the power spectrum of $f\prime(m)$ displays a narrow peak at the fringe frequency. However, any of these operations decreases the SNR and the Fourier transform shows noisy components of higher frequencies. These computations introduce important noise levels in the far wings of $f(m)$ where it is low-valued. In addition, the Fourier transform of the rectangular window shows important sidelobes. The, if the frequency of the fringes is not too low, it is more convenient to decrease the noise and the importance of the sidelobes than to minimize the linewidth. This can be achieved by multiplying $\log f(m)$ or $f\prime(m)$ by a window function (for example, a Hanning window) having a low value near the extremities of the interval and showing very weak sidelobes.

The advantage of the one dimensional averaging technique is rapidity. The computation is completed in a few seconds, typically 1-2 sec, using the Micro VAX II computer.

The main disadvantage is that it requires the input of an operator making it slow and prone to error, i.e., wrong input of the fringe orientation angle. The possibilites of making this approach fully automated, e.g. by incorporating some means of an automatic search of the fringe orientatin are not promising. The difficulty resides on the fact that the fringes contain a large amount of speckle noise, and that great uncertainty would be associated with any scheme for the automatic angle search.

6.1.2. Fully automated approaches

A logical response to the difficulties which are encountered using the previous data reduction scheme is the use of fuel two-dimensional processing techniques to determine the periodic component of the fringes, and their orientation. Two methods seem attractive: (i) the full two-dimensional autocorrelation and its counterpart (ii) the full two-dimensional Fourier transform of the fringes intensity distribution. In both cases one world be interested in determining the location of the maxima. However, considering that the Young's fringes data consist of a large matrix (typically 512 x 512 format) these schemes are com-

putationally heavy and may be quite slow.

A fully automated method based on the autocorrelation computed along a limited number of independent directions has been developed. The principle of this method is as follows:

Each line of the picture can be considered as a noisy periodic signal with variable phase, the automatic determination of a velocity component can be performed only by averaging over a quantity independent of the phase. The autocorrelation for each line or its Fourier transform for the power spectrum satisfies this requirement.

The m velocity component can be computed from:

$$g(u) = \sum_{n=0}^{511} \left[\frac{\sum_m [I(m,n)I(m+u,n)]}{\sum_m [I(m,n)]_2} \right] - 511 < u < 511 \qquad (44)$$

This algorithm has been implemented using the (DVP) pipeline processor of the Gould IP-8500 image processor to perform simultaneously the autocorrelation for the entire image.

The averaged autocorrelation $g(u)$ exhibits an important peak centered $u = 0$ which is mainly due to the speckle present in the fringes. The height of this peak can be decreased by constructing

$$g^1(u) = \frac{g(u)}{[1 + exp(-u^2/p^2)]} \qquad (45)$$

where p is an adjustable parameter. As a result, the resolution of the peaks of the power spectrum of $g^1(u)$ is improved.

By computing the averaged autocorrelation of the columns of $I(m,n)$, the n component of the velocity component can be computed. However, in order to determine the velocity vector, with accuracy, one needs to compute at least four components. From these the velocity vector is determined by selecting the values of the components which have been computed from autocorrelation having the highest SNR, and visibility.

The price to be paid for automation is an increase in computation time. In our configuration, the determination of the velocity vector requires 3-4 sec. However, this algorithm has been implemented in a newer and faster processor with a time performance which is about 20 times faster.

A shortcoming of the autocorrelation technique is the difficulty to measure the velocity when the fringe density is too low (less than five bright fringes, including the central one). In this case, the velocity can often be evaluated by the interactive one dimensional averaging method. So, the two methods are complementary.

List of figures

1. Basic set-up to generate specklegram.
2. Schematic diagram of Young's fringe formation for specklegram analysis.
3. Schematic of experimental set-up for laser speckle velocimetry in fluids.
4. Young's fringes
5. Set-up for observing the photographic plate with a spatial filter.
6. Young's fringes generated by:
7. Variation of fringe width number of exposures.
8. Typical density-exposure curve for a film.
9. Schematic of imaging system estimating the effect of out-of-plane motion.
10. Schematic for the simultaneous recording of two double exposure photographic plates to measure the three components of displacement.
11. Set-up for fringe analysis.

LIST OF REFERENCES

1. Gharib, M., Hernan, M.A., Yavrouian, A.H., and Saroia, V., "Flow Velocity Measurement by Image Processing of Optically Activated Tracers", AIAA Paper 85-0172, 1985.

2. Dimotakis, P.E., Debussy, F.D., and Koochestahani, M.M., "Particle Streak Velocity Field Measurements in a Two-Dimensional Mixing Layer", *Phys. Fluids*, Vol. 24, 1981, pp. 995-999.

3. Kobaybashi, T., Ishihara, T., and Sasaki, N., "Automatic Analysis of Photographs of Trace Particles by Microcomputer System", 3rd Int. Conf. Flow Vis., Ann Arbor, USA, 1983, pp. 261-265.

4. Frish, M.B. and Webb, W.W., "Direct Measurement of Vorticity by Optical Probe", *J. Fluid Mech.*, Vol. 107, 1981, pp. 173-200.

5. Erf, R.K., "Application of Laser Speckle to Measurement", *Laser Applications*, Vol. 4 (ed. by Goodman, J.W. and Ross, M.), Academic Press, 1980.

6. Stetson, K.A., "A Review of Speckle Photography and Interferometry", *Opt. Engr.*, Vol. 14, 1975, pp. 482-489.

7. Collicott, S.H. and Hesselink, L., "Anamorphic Optical Processing of Laser Speckle Anemometer Data", *Bull. Amer. Phys. Soc.*, Vol. 30, No. 10, 1985, p. 1728.

8. Simpkins, P.G. and Dudderar, T.D., "Laser Speckle Measurements of Transient Bernard Convection", *J. Fluid Mech.*, Vol. 89, 1978, pp. 665-671.

9. Meynart, R., "Speckle Velocimetry Study of Vortex Pairing in a Low-Re Unexcited Jet", *Phys. of Fluids*, Vol. 26, 1983, pp. 2074-2079.

10. Meynart, R., "Instantaneous Velocity Field Measurements in Unsteady Gas Flow by Speckle Velocimetry", *Appl. Opt.*, Vol. 22, 1983, pp. 535-540.

11. Lourenco, L.M., "Velocity Measurement by Optical and Digital Processing of Time Exposed Particle Pairs", *Bull. Amer. Phys. Soc.*, Vol. 29, 1984, pp. 1531.

12. Lourenco, L.M. and Whiffen, M.C., "Laser Speckle Methods in Fluid Dynamics Applications". Proc. Int. Symp. on Appl. of Laser Anemometry to Fluid Mechanics,

Lisbon, Portugal, 1984.

13. Adrian, R.J. and Yao, C.S., "Pulsed Laser Technique Application to Liquid and Gaseous Flows and the Scattering Power of Seed Materials", *Appl. Opt.*, Vol. 24, 1985, pp. 44-52.

14. Jacquot, P. and Rastogi, P.K., "Influence of Out-of-Plane Deformation and its Elimination in White Light Speckle Photography", *Opt. Lasers in Engng*, Vol.2, 1981, pp. 33-55.

15. Yao, C.S. and Adrian, R.J., "Orthogonal Compression and I-D Analysis Technique for Measurement of 2-D Parcile Displacements in Pulsed-Laser-Velcimetry", *Appl. Opt.*, Vol. 23, 1984, pp. 1687-1689.

16. 16. Meynart, R., "Equal Velocity Fringes in a Rayleigh-Benard Flow by a Speckle Method", *Appl. Opt.*, Vol. 19, 1980, pp. 1385-1386.

17. Lourenco, L.M. and Meynart, R., "Laser Speckle Velocimetry in Fluid Dynamics Applications", *V.K.I. L.S. Digital Image Processing in Fluid Dynamics*, 1984.

18. Lourenco, L.M., Krothapalli, A., Buchlin, J.M., and Riethmuller, M.L., "A non-invasive technique for the measurement of velocity and vorticity fields", paper for publication in the *AIAA Journal*.

19. Adrian, R.J., private communication.

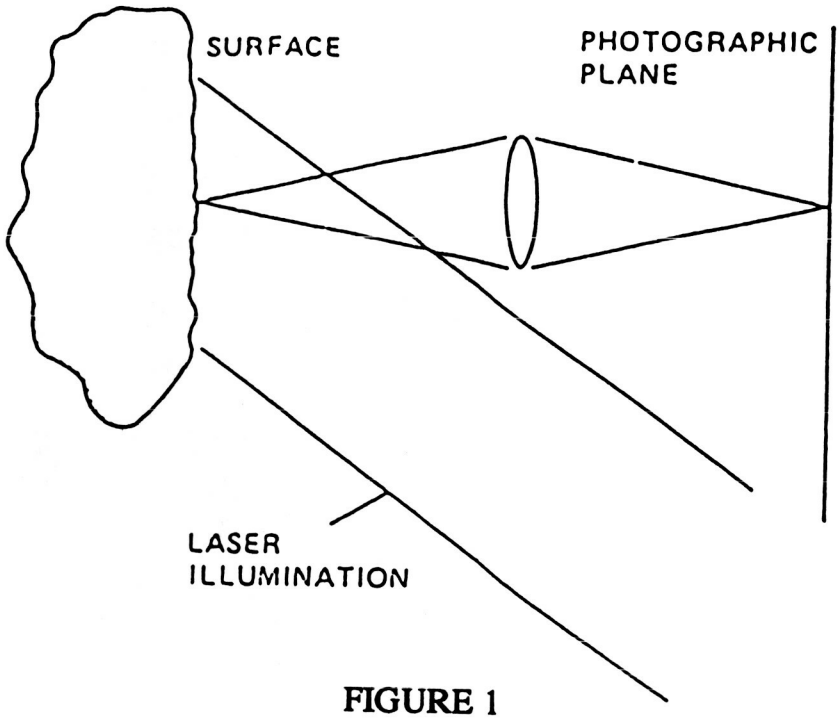

FIGURE 1

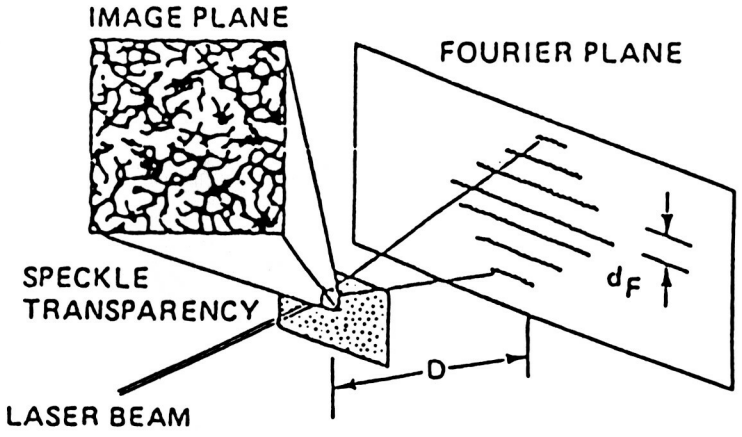

FIGURE 2

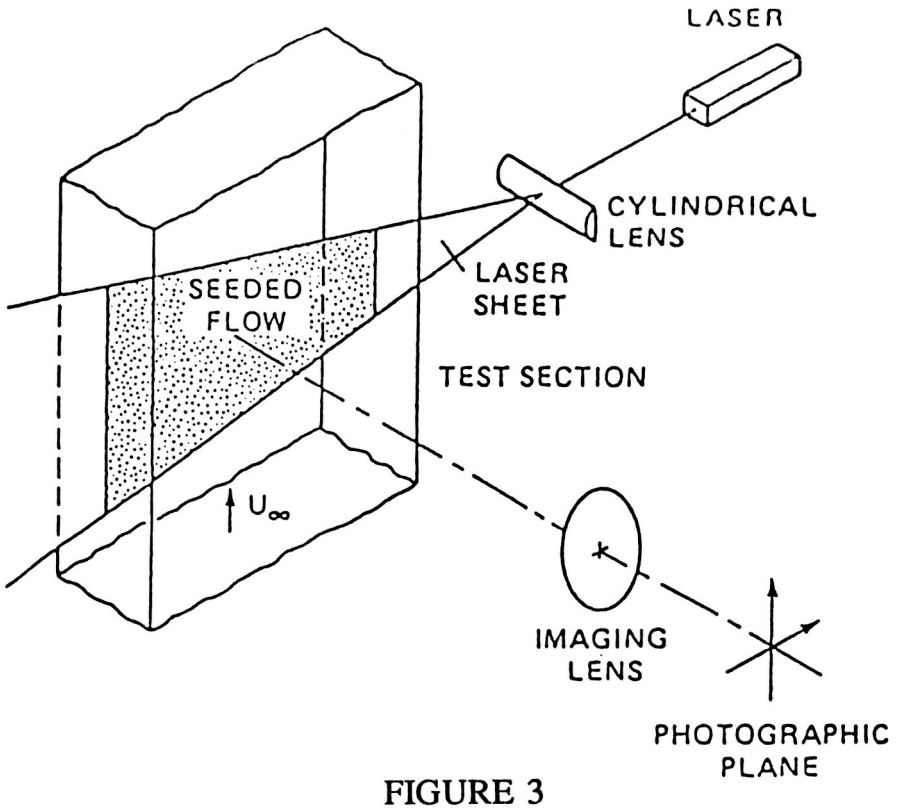

FIGURE 3

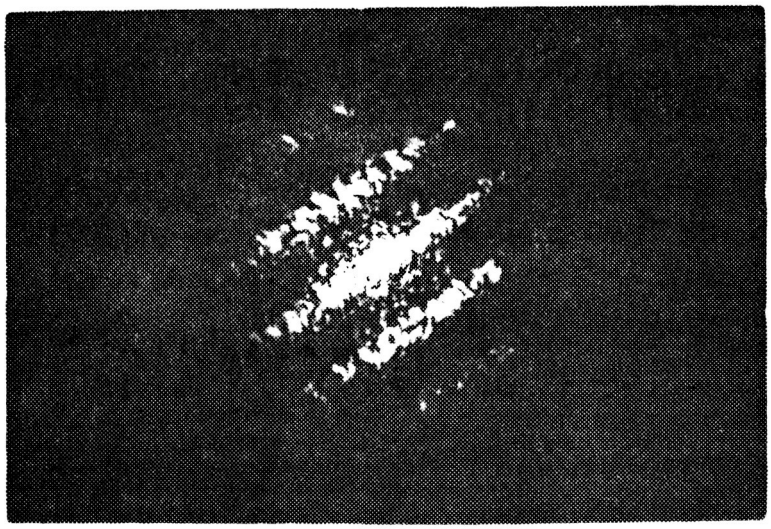

FIGURE 4

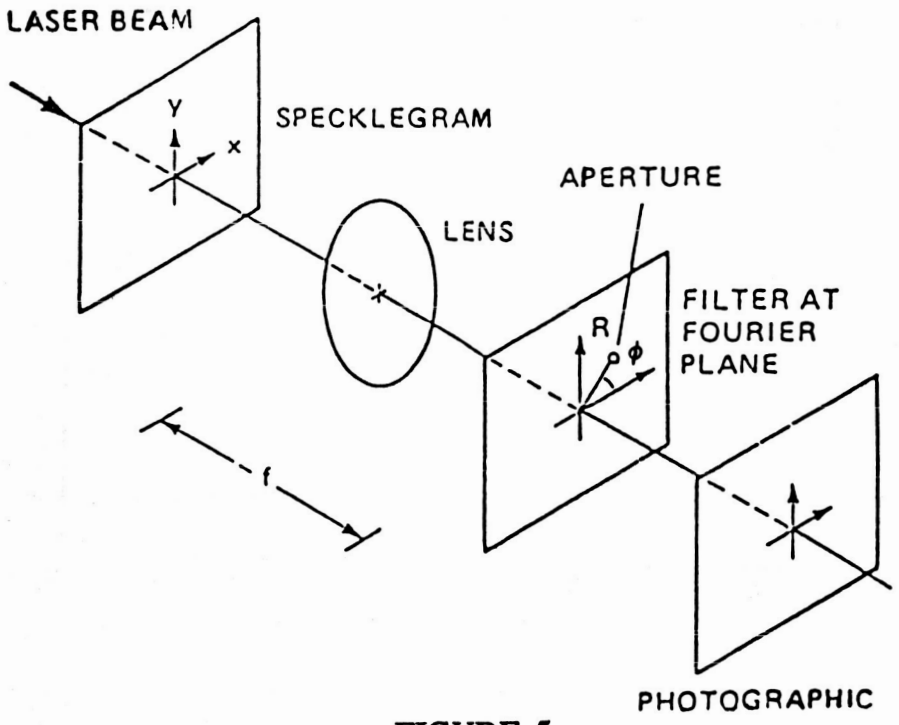

FIGURE 5

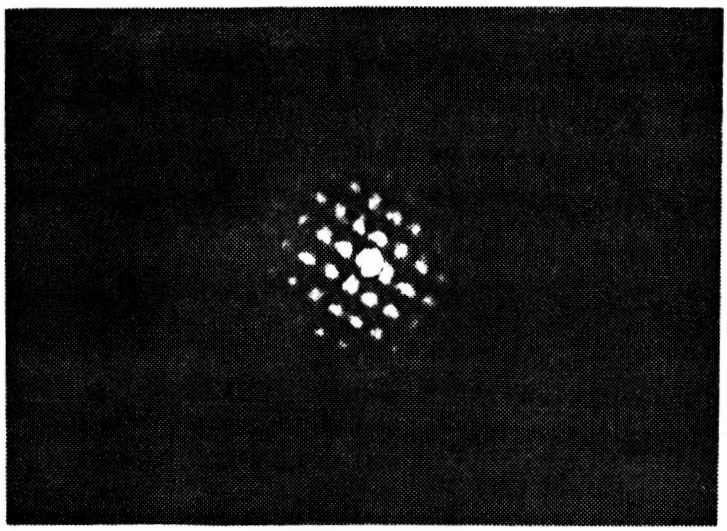

FIGURE 6

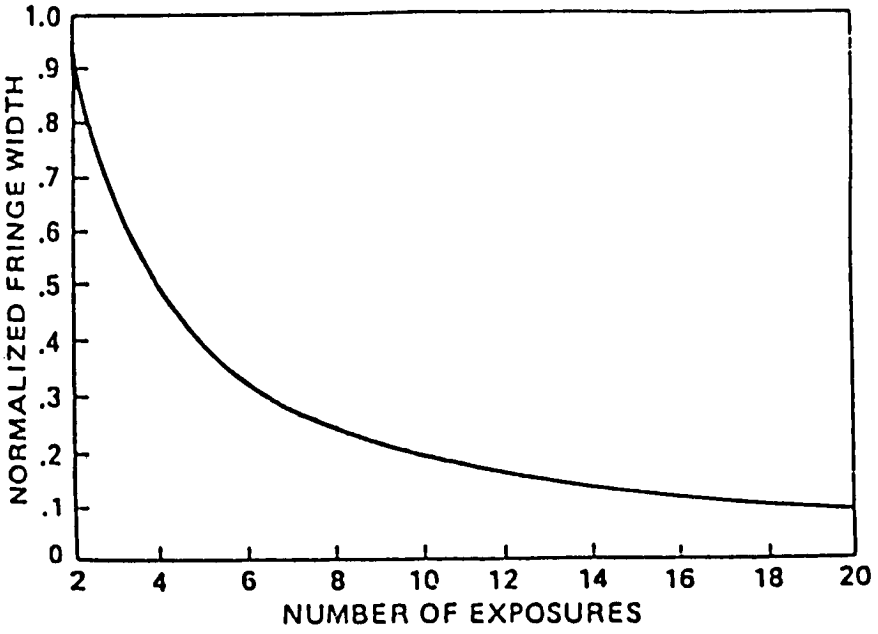

FIGURE 7

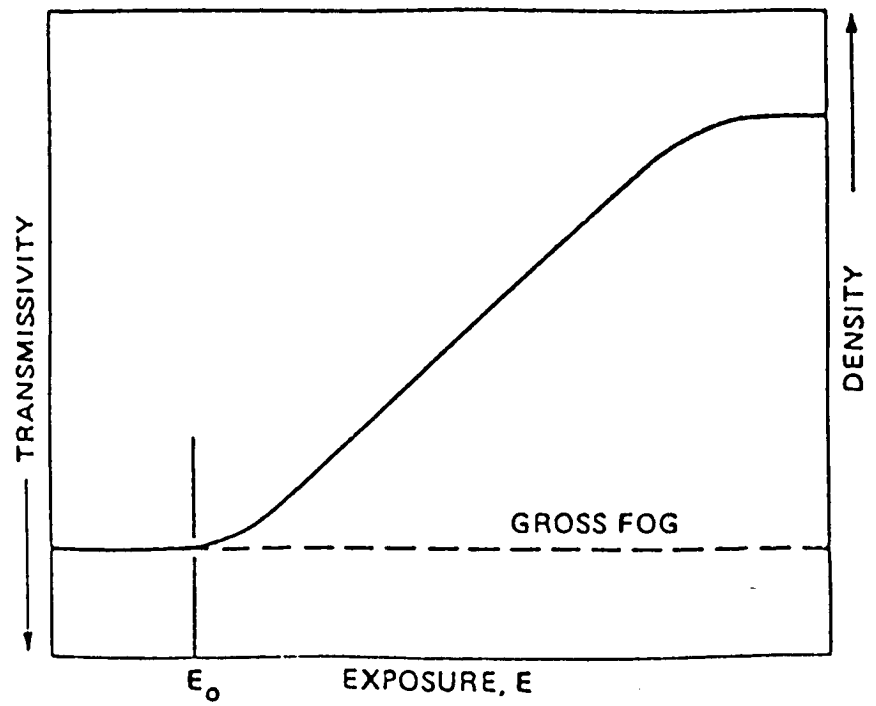

FIGURE 8

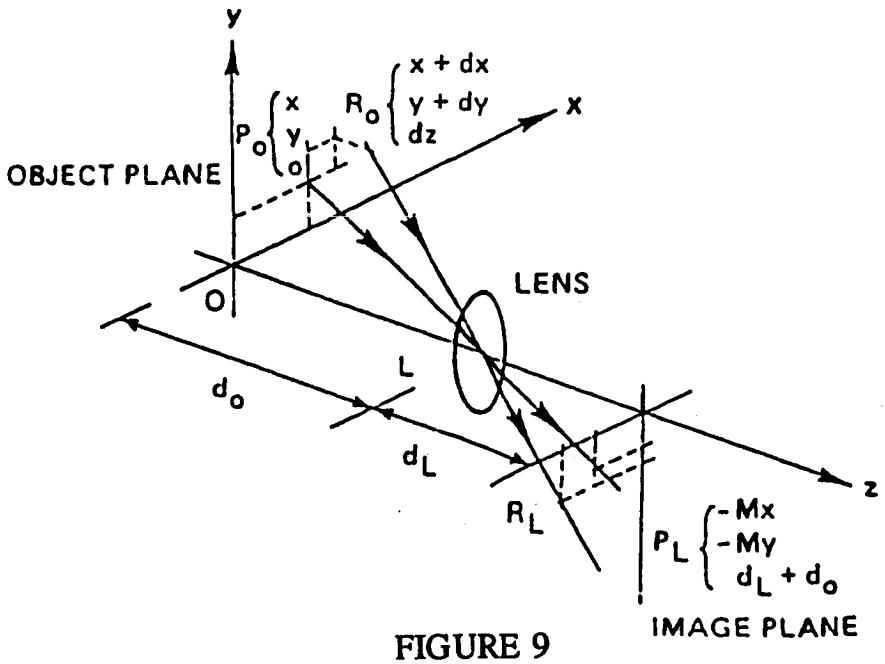

FIGURE 9

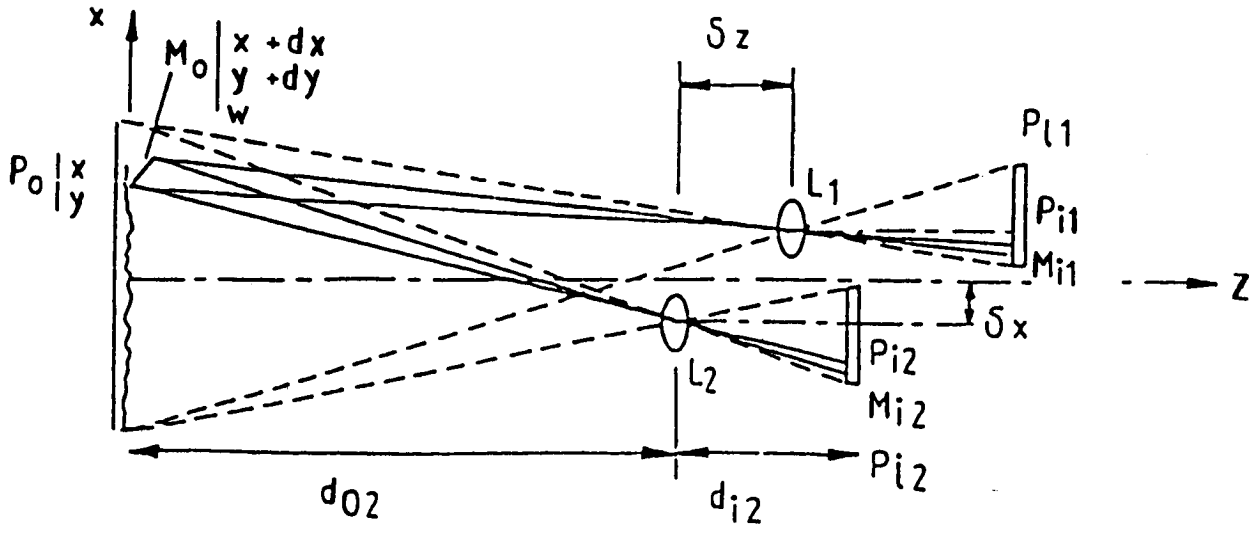

FIGURE 10

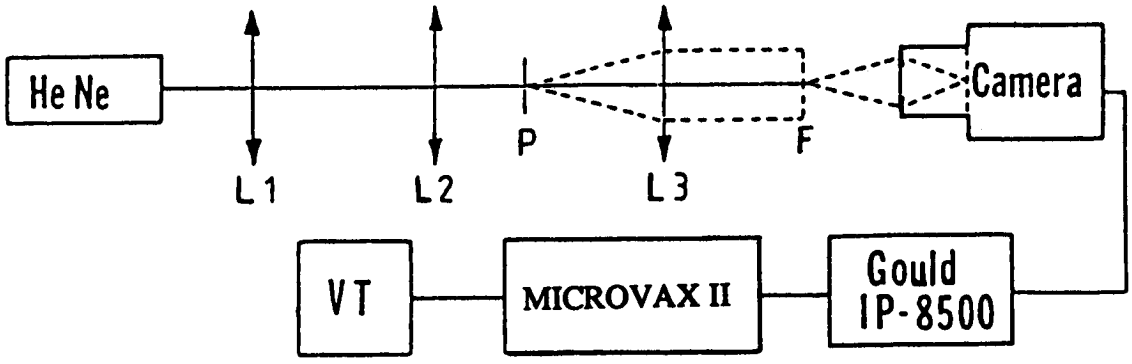

FIGURE 11

APPLICATIONS

PAPER

APPENDIX ? - YES

A Non-invasive Experimental Technique for the Measurement of Unsteady Velocity and Vorticity Fields

L. Lourenco and A. Krothapalli
Florida State University, Tallahassee, Florida
and
J.M. Buchlin and M.L. Riethmuller
von Karman Institute for Fluid Dynamics
Rhode-St-Genese, Belgium

SUMMARY

A new velocity measurement technique is described that provides the simultaneous visualization of a two-dimensional streamline pattern and the quantification of the velocity field. The main advantage of this technique is that the velocity field can be measured with sufficient accuracy and spatial resolution so that the vorticity field can be readily obtained. This technique is ideally suited for the study of unsteady vortical flows, which occur in high angle of attack aerodynamics. The technique, some of the important parameters that affect its use, and some recent examples are described.

NOMENCLATURE

C	airfoil chord
d	cylinder diameter
Re	Reynolds number
t	time
U	streamwise velocity
V	lateral velocity
Δx	streamwise distance between scanning locations
Δy	lateral distance between scanning locations
Ω	vorticity

1. INTRODUCTION

Since the early works of Prandtl water facilities together with flow visualization techniques e.g. dye injection, hydrogen bubbles, have been extensively used to provide a better understanding of complex flow phenomena, such as the ones occurring in high angle of attack aerodynamics. The advantage that water facilities have over conventional wind tunnels is that they provide an easy means to perform the flow visualization. In particular, when dealing with unsteady flows, because of the lower kinematic viscosity of water compared to that of air, it is possible to reproduce an aerodynamic flow in water with a lower free stream velocity to attain a Reynolds number comparable to that in air. Due to the lower velocities, the flow time scales become relatively larger thus leading to clearer observations of dynamic phenomena.

Even though conventional visualization techniques are an excellent means to understand the global flow features, they only provide qualitative information. A detailed description of flow fields can only be achieved through mapping of the entire flow field. However, the measurement of velocity in unsteady flows remains a challenging problem in experimental fluid mechanics. Available techniques such as hot-wire anemometry and Laser Doppler Velocimetry can only provide "one point" information. In order to obtain whole field data, measurements must be carried out sequentially one point at a time. Although this sequential method can be easily implemented in applications involving steady flows, it is of rather difficult application in unsteady flow phenomena.

Recently, a novel measurement technique commonly known as Laser Speckle or Particle Image Displacement Velocimetry became available. This technique permits the simultaneous visualization of the two-dimensional streamline pattern in unsteady flows and the quantification of the velocity field. The main advantage of this new technique is that the whole two-dimensional velocity field can be recovered with great accuracy and spatial resolution, from which the instantaneous vorticity field can be easily obtained. This constitutes a great asset for the study of a variety of flows that evolve stochastically in both space and time, and in the case of interest, to the study of unsteady separated flows, which occur in high angle of attack aerodynamics.

2. PRINCIPLE OF THE TECHNIQUE

The application of LSV or PIDV to fluid flow measurement involves several steps. First, it is necessary to "create" a selected plane or surface within the flow field. This is accomplished by seeding the flow with small tracer particles, similarly to LDV applications, and illuminating it with a sheet of coherent light, as shown in Figure 1. A pulsed laser such as a Ruby or a NdYag laser, or a CW laser with a shutter is normally used as the light source. The laser sheet is formed, for example, by focusing

the laser beam first with a long focal length spherical lens, to obtain minimum thickness, and then diverging the beam in one dimension with a cylindrical lens. The light scattered by the seeding particles in the illuminated plane provides a moving pattern. When the seeding concentration is low, the pattern consists of resolved diffraction limited images of the particles. When their concentration increases, the images overlap and interfere to produce a random speckle pattern. A multiple exposure photograph records this moving pattern. The lower particle concentration originates a mode of operation of the technique referred to as Particle Image Displacement Velocimetry, reserving the term Laser Speckle Velocimetry for the high particle concentration levels where a random speckle pattern is actually formed (reference 1). In a second step the local fluid velocity is derived from the ratio of the measured spacing between the images of the same tracer, or speckle grain, and the time between exposures.

Several methods exist to convert the information contained in the multiple-exposed photograph, or specklegram, to flow field data such as velocity or vorticity. The recorded image, whether formed by isolated disks, in the case of low particle concentration, or speckle grains for high particle concentration is a complicated random pattern. It would be very difficult to measure the local displacements by visual or computer-aided inspection. However, it is important to realize that the multiple exposure photograph results in a periodic random image from which the periodicity information can be retrieved using Fourier or Auto-correlation analysis. Basically, the multiple-exposed photographs or specklegrams can be analyzed either on a point-by-point basis, which yields measurements of the local displacements (velocity), (refs. 2-3) or with a whole field filtering technique, which yields isovelocity contours (ref. 3). The method, which has been selected and implemented by the Fluid Mechanics Research Laboratory at the Florida State University, is the Young's fringes method. The local displacement is determined using an focused laser beam to interrogate a small area of the multiple exposed photograph transparency. The diffraction produced by coherent illumination of the multiple images in the negative generates Young's fringes, in the Fourier plane of a lens, provided that the particle images correlate. This is shown schematically in Figure 2. These fringes have an orientation which is perpendicular to the direction of the local displacement and a spacing inversely proportional to the displacement. The use of Young's fringes eliminates the difficulties of finding the individual image pairs in the photograph. The basis of the Young's fringe method is described in reference 3.

3. DIRECTION SENSITIVITY AND DYNAMIC RANGE

The photographic recording method discussed above has the disadvantage that the photograph consists of a sequence of multiple particle images which have a 180° ambiguity in the direction of the velocity vector. In addition, it has been shown (reference 4) that the velocity dynamic range of the technique is limited to a maximum

value of about 10. In most flows of interest (e.g. boundary layers and separated flows), this dynamic range is not sufficient to capture the flow field in its entirety. These limitations are critical when measuring complex flows having flow reversals and stagnation areas.

A method to resolve both the ambiguity of the velocity vector as well as to improve the technique's velocity range is incorporated in this experiment. This method, commonly known as "velocity bias technique", consists of recording the flow field in a moving reference frame, thus superposing a known velocity bias to the actual flow velocity. This effect may be accomplished in several ways, in particular, using a moving camera during the photographic recording or by optical means using scanning or rotating mirrors. The method which is currently employed uses a scanning mirror to displace the image during the exposure with a predetermined velocity. A schematic of the scanning mirror arrangement is shown in figure 3. Consider two particle pairs A_0B_0 and C_0D_0 having equal displacements in opposite directions in the object plane. By introducing a mirror placed at 45° between the camera lens and the object plane, the corresponding displacements appear in the film plane as AB and CD with equal magnitudes. When the mirror is rotated by an angle of $\Delta\theta$ between exposures, the displacements corresponding to A_0B_0 and C_0D_0 appear in the film plane as AB^1 and CD^1 with different magnitudes. The correct displacement or velocity with its direction can now be obtained upon removal of the velocity bias.

4. VALIDATION OF THE TECHNIQUE

4.1 Experimental configuration

The capabilities of the present technique are evaluated in a measurement of the transient flow over a NACA 0012 at high incidence, and the near-wake flow development behind a circular cylinder impulsively accelerated to constant velocity. Both flows were created by towing models in the reduced scale Fluid Mechanics Research Laboratory towing tank facility. The tank is 300 x 300 x 600mm. A detailed examination showed that the motion of the carriage is smooth and vibration free. In this facility, the towing carriage is driven by a variable D.C. motor, and the towing velocity can vary from 0 to 100mm/sec. For the photography a 35mm camera (NIKON F-3) is used. In order to photograph the flow at regular time intervals, the photographic camera is equipped with an electric winding device. The photographic time interval available with this camera can be continuously varied up to a maximum of 6 frames per second. Two options are available to fix the camera; one by attaching it to the towing carriage, which means an observation point fixed in relation to the model, and the other by attaching it to the frame of the water tank, which means an observation point fixed in relation to the fluid.

The NACA 0012 airfoil is 60mm in chord and at 30° incidence; the circular cylinder is 25.4mm in diameter. Both models were towed with a velocity of 23.5mm/sec. The fluid used in these experiments was water seeded with 4μm metallic coated particles (TSI model 10087). The corresponding Reynolds numbers were 1400 for the airfoil and 550 for the cylinder. These flows are excellent test cases because they include large scale vortical motions and extreme velocity gradients. These extreme gradients serve as a test to the technique's capabilities of providing information over a large velocity range.

For the illumination, a laser beam from a 5 watt Argon-Ion Laser (Spectra-Physics model 2000) is steered and focused to a diameter of .3mm using an inverse telescope lens arrangement. A cylindrical lens, with a focal length of -6.35mm, is used to diverge the focused beam in one dimension, creating a laser sheet. The laser sheet is 70mm wide and illuminates the mid-span section of the models. For the multiple exposure, the CW laser beam is modulated using a Bragg cell. In this experiment, the laser power density of the sheet was 0.27W/m^2. In order to record the time development of the flow field, the camera is attached to the towing carriage. The aperture of the camera lens with a focal length of 50mm and a spacer of 12mm, is set at F# 5.6 and the magnification is 0.40. The film used in these experiments was a Polaroid Polagraph with a sensitivity of 400 ASA and a resolution of about 80 lines/mm. This resolution proved to be sufficient to accurately record the flow field. The advantages in the use of Polaroid film are (i) easy and fast processing of the film (ii) because the Polaroid Polagraph is a positive film it saves the need for contact printing of film negatives, prior to analysis, in order to increase the SNR of the data (ref. 1).

5. RESULTS

5.1 Flow past the NACA 0012 airfoil

Figure 4(a) is a multiple exposed photograph of the flow past an impulsively started airfoil captured at a stage of its development corresponding to non-dimensional time $t^*=t\frac{U}{C}=1.5$, with t the time from start-up, U the free stream velocity and C the airfoil chord. This figure depicts the complexity of the flow field which exhibits large areas of flow reversal and stagnation regions. Analysis of this film transparency would provide the velocity vector information within the restriction mentioned above, i.e., with an 180° ambiguity in direction of the velocity vector and regions of drop-out where the flow velocity is less than the lower velocity range limit of the technique. Instead, the "velocity bias technique" is used and a "biased" image is recorded and analyzed (fig. 4(b)).

The velocity data is acquired in a square mesh by digital processing of the Young's fringes, produced by point-by-point scanning of the Polaroid transparency. The scanning step size an the dimension of the analyzing beam are 0.5mm, which corresponds

to a spatial resolution of about 1.25mm in the object plane or about $\frac{1}{50}$ chord of the airfoil. The resulting velocity field is presented in figure 5(a). The actual velocity field in the reference frame of the airfoil is presented in figure 5(b). This data is recovered upon removal of the velocity bias, which is, for this particular experiment, equal to 2 times the free-stream velocity.

5.2 Near-wake flow behind a circular cylinder

Similarly the flow behind a circular cylinder was captured at several stages of its development corresponding to t*, the non-dimensional time based on the cylinder diameter, between 0.6 and 5.2. Figures 6(a) to (f) are the measured velocity fields, and consist of a good representation of the expected flow pattern. In these figures, the length of each vector is proportional to the local velocity at that point. Because of the high spatial resolution of these data, vorticity can be derived by taking spatial derivatives. Letting each grid location be labeled with indices, i, j, the z-vorticity component at location (i,j) is

$$\Omega_{i,j} = \frac{1}{2}\left[\frac{V_{i+1,j} - V_{i-1,j}}{2\Delta x} - \frac{U_{i,j+1} - U_{i,j-1}}{2\Delta y}\right]$$

where Δx and Δy are the mesh intervals in the streamwise and cross-stream direction, respectively. For convenience, the vorticity data normalized with respect to the free stream velocity and cylinder diameter, is displayed by color coding of each velocity vector. The color code represents the vorticity level, the magnitude of which is given by the color bar on the top of each figure. The red and blue colors represent the peak positive and negative vorticity regions respectively.

6. CONCLUSIONS

A recently developed velocity measurement technique, known as Particle Image Displacement Velocimetry has been briefly described. Using this technique rather complex time varying flow fields can be captured and analyzed with great detail. The potential of the technique is illustrated using two flow fields as test cases: Flow past an airfoil and behind a circular cylinder.

The technique has been shown to provide both flow visualization and quantitative measurements, which include velocity and vorticity fields.

REFERENCES

1. Lourenco, L.; and Krothapalli, A.: The role of photographic parameters in laser speckle or particle image displacement velocimetry". Experiments in Fluids, vol. 5, 1987, pp. 29-32.

2. Yao, C.S.; and Adrian, R.J.: Orthogonal compression and 1-D analysis technique for measu ement of 2-D particle displacements in pulsed laser velocimetry. Applied Optics, vol. 23, 1984, pp. 1667-1689.

3. Lourenco, L.; and Meynart, R.: Laser speckle velocimetry in fluid dynamics applications. VKI Lecture series 1984-03, Digital Image Processing in Fluid Dynamics, Belgium, 1984.

4. Lourenco,L.; Krothapalli, A.; Buchlin, J.M.; and Riethmuller, M.L.: Non-invasive experimental technique for the measurement of unsteady velocity fields. AIAA Journal, vol. 24, 1986, pp. 1715-1717.

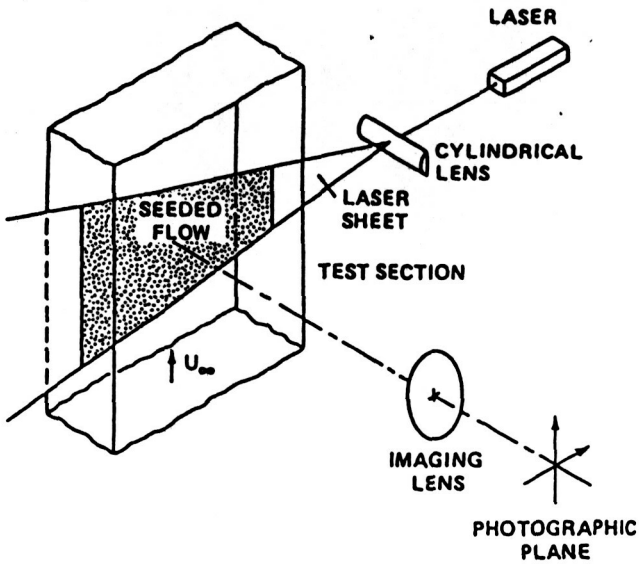

Figure 1. Schematic Arrangement for the Photographic Recording.

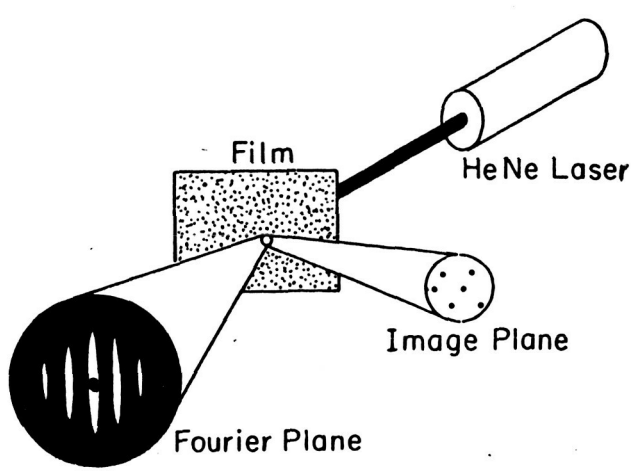

Figure 2. Schematic Arrangement for obtaining Young's Fringes

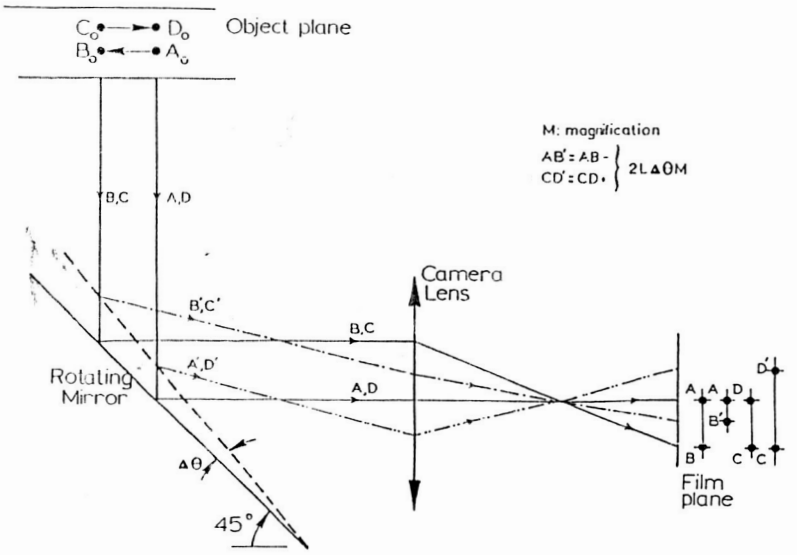

Figure 3. Scanning Mirror Arrangement for Velocity Bias.

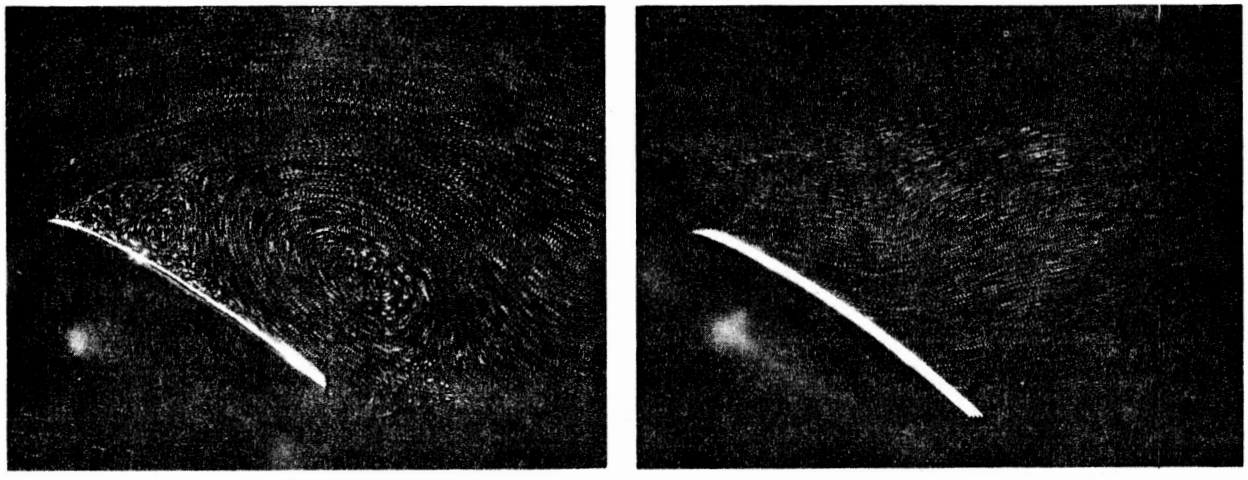

(a) (b)

Figure 4. Multiple Exposed Photograph a) Unbiased Image; b) Biased Image

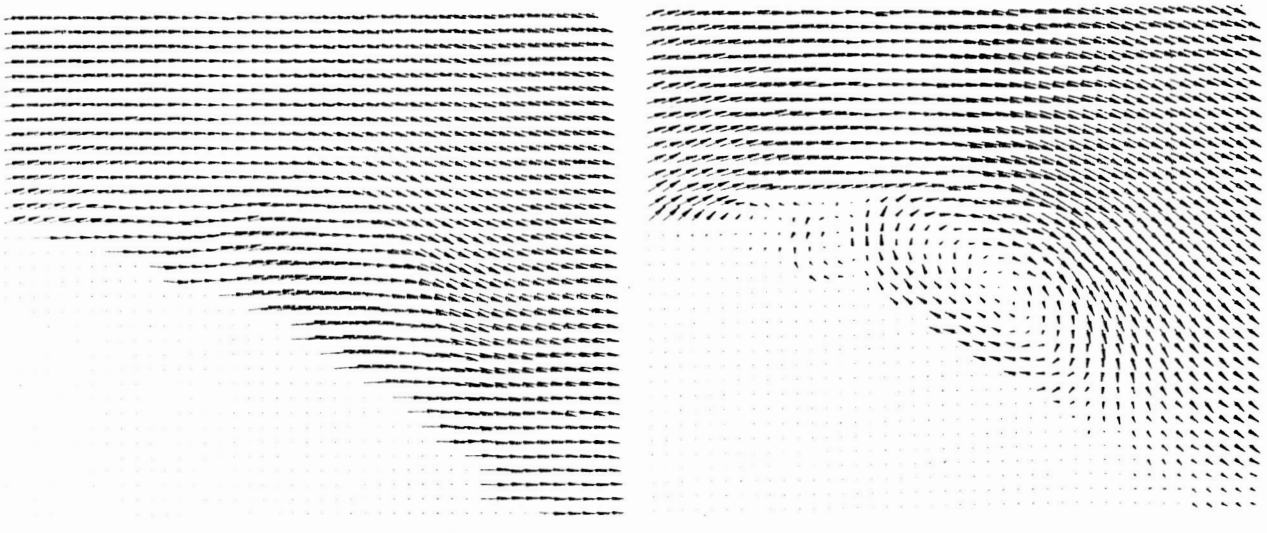

(a) (b)

Figure 5. Instantaneous Velocity Field a) Before Removal of Velocity Bias; b) After Removal of the Velocity Bias.

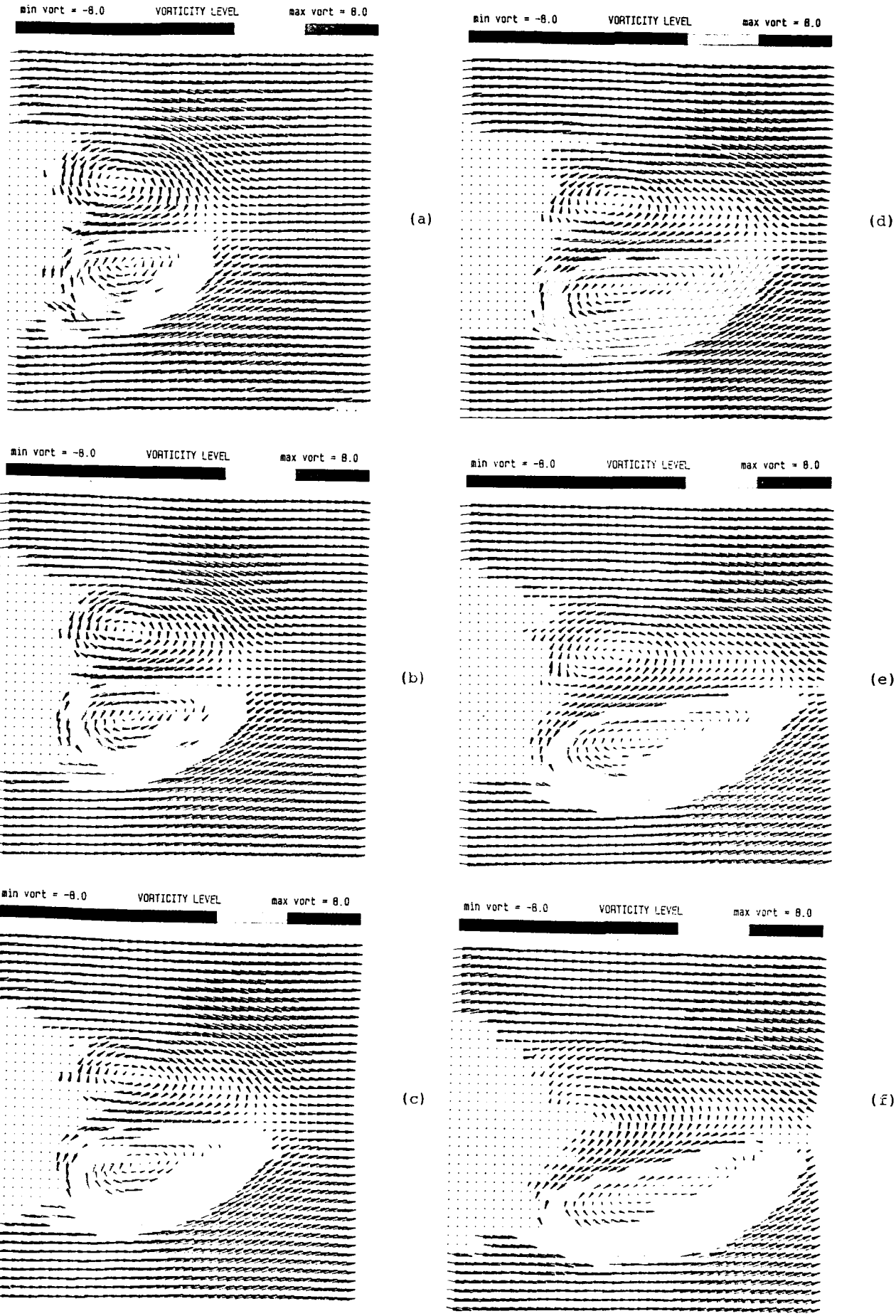

Figure 6. Velocity and Vorticity Field of the Wake Flow; a) t^*=2.2; b) t^*=2.7; c) t^*= 3.2; d) t^*=3.7; e) t^*=4.2; f) t^*=4.7.

LETTERS

The purpose of this Letters section is to provide rapid dissemination of important new results in the fields regularly covered by The Physics of Fluids. Results of extended research should not be presented as a series of letters in place of comprehensive articles. Letters cannot exceed three printed pages in length, including space allowed for title, figures, tables, references and an abstract limited to about 100 words. There is a three-month time limit, from date of receipt to acceptance, for processing Letter manuscripts. Authors must also submit a brief statement justifying rapid publication in the Letters section.

Particle image displacement velocimetry measurements of a three-dimensional jet

L. Lourenco and A. Krothapalli
Department of Mechanical Engineering, Florida A&M University/Florida State University College of Engineering, P.O. Box 2175, Tallahassee, Florida 32316-2175

(Received 19 February 1988; accepted 22 April 1988)

A whole field experimental technique, commonly referred to as particle image displacement velocimetry (PIDV), is used for the measurement of the instantaneous two-dimensional velocity fields in the transition region of a three-dimensional jet issuing from a rectangular nozzle with aspect ratio 4. The experiments were performed using an air jet at a Reynolds number based on the hydraulic diameter of 3600. The rollup of the laminar shear layer into vortices and their subsequent interactions are examined.

Particle image displacement velocimetry (PIDV) is an attractive experimental technique for the nonintrusive measurement of two-dimensional velocity fields in free shear layers dominated by quasideterministic large structures. It provides an instantaneous velocity field measurement capability with good spatial resolution, from which the vorticity field can be computed accurately.

Earlier investigations[1,2] have been carried out using a technique similar to PIDV to study the mixing region of an axisymmetric jet. However, as a result of the limited dynamic range in the velocity measurements[1] or limited spatial coverage of the flow field,[2] a number of important features of the vortical structures could not be obtained. The purpose of this Letter is to establish the validity and attractiveness of the PIDV technique for accurate measurements of the instantaneous two-dimensional velocity field in a three-dimensional, time dependent, vortical, and entraining flow.

The flow field considered is a three-dimensional incompressible jet of air issuing from a rectangular nozzle of aspect ratio 4. The structure and development of such a jet is markedly different from those issuing from two-dimensional and axisymmetric nozzles.[3] One of the interesting features is the "crossover" phenomenon, which is generally characterized by the switching of the major and minor axes downstream of the nozzle exit. The physical mechanism of this phenomenon is not well understood. Recent experiments on low-aspect-ratio elliptic jets[4] suggest that an initial instability process may influence the position of the crossover point and thus the development of the jet. With this in mind, the present investigation focuses on studying the structure and growth of the mixing layer region of the jet.

A brief description of the particle image displacement velocimetry technique is given here, however, for more details see Refs. 5 and 6. The PIDV measurements of fluid flows can be described as follows: A selected cross section of the flow is illuminated by a sheet of coherent light. A pulsed laser such as a Nd:Yag laser, is normally used as the light source. The laser sheet is formed by focusing the laser beam with a spherical lens of long focal length followed by a one-dimensional expansion using a cylindrical lens. Within the illuminated sheet, the flow is made visible through small tracer particles seeded within the fluid. The illuminated particles generate resolved diffraction limited images recorded in a multiple exposure photograph. The spacing between the images of the same tracer provides a measure of the local flow velocity.

To determine this spacing, a Fourier analysis is used. A focused laser beam is used to interrogate a small area of the multiple exposure photograph transparency. The diffraction produced by coherent illumination of the multiple images in the film transparency generates Young's fringes. The fringes are oriented perpendicular to the direction of the local displacement and their spacing is inversely proportional to the magnitude of the displacement. The use of Young's fringes avoids the difficulty of locating individual image pairs in the photograph.

In this method, the sign of the velocity cannot be determined.[7] A method to resolve this ambiguity, as well as to improve the technique's capabilities to measure large velocity gradients, is incorporated in this experiment. This method,[7,2] commonly known as the "velocity bias technique," consists of recording the flow field in a moving reference frame, thus superposing a known velocity bias to the actual flow velocity. This effect may be accomplished in several ways, such as using a moving camera during the photographic recording or by optical means using scanning or ro-

 0031-9171/88/071835-03$01.90

tating mirrors. For the data presented here, a scanning mirror is used to displace the image during the photographic recording.

A simple low speed air supply system was used to flow air into a cylindrical settling chamber 27 cm in length and 10 cm in diameter. A honeycomb and a series of screens at the inlet of the nozzle are used to further reduce flow disturbances. The cross-section area of the contraction changes gradually from a circular cross section, 10 cm in diameter, to a rectangular nozzle. The long dimension and the short dimension of the rectangular nozzle are, respectively, 3 cm and 0.75 cm and the streamwise contours of the contraction for the two central planes are fifth-order polynomials. In order to obtain appropriate jet seeding, smoke particles in the submicron range are produced using a Rosco-type 1500 smoke generator. The smoke and ambient air are mixed in a large cylindrical settling tank (100 cm in length and 45 cm in diameter). The air–smoke mixture is then supplied to the settling chamber of the jet using a small axial fan. A second smoke generator of the same type is used to seed the outside ambient fluid surrounding the jet.

A mean velocity of 4.5 m/sec is maintained at the exit plane of the nozzle; the mean velocity profile at the exit plane is flat with a laminar boundary layer at the walls. The Reynolds numbers based on the hydraulic diameter and the small dimension of the nozzle are, respectively, 3600 and 2250.

For the illumination, a laser beam from a frequency-doubled, double-pulsed Nd:Yag laser (Spectra-Physics model DCR-11) is steered and focused to a diameter of 0.3 mm using an inverse telescope lens arrangement. A cylindrical lens with a focal length of -24.5 mm diverges the focused beam one dimensionally, creating the light sheet. The laser sheet is 45 mm wide and illuminates the central plane through the small dimension of the nozzle. A 35 mm camera (Nikon F-3) with a 150 mm macro lens loaded with 400ASA KODAK TMAX film, a film with good sensitivity at the laser light frequency, is used for the photographic recording. The lens aperture is set at $f/5.6$ and the magnification is 0.5. Two laser pulses with a duration of 10 nsec and a separation of 50 μsec are used for the double exposure recording. In this mode, the laser delivered a 15 mJ/pulse of light at the 0.532 nm wavelength. The pulse separation of 50 μsec is much smaller than any relevant time scale of the flow field, thus the double exposure photograph truly represents a flow field at a given instant of time.

The analysis of the photograph was performed by means of an integrated image analysis system based on a Gould IP-8500 digital image processor controlled by a μVAX II. The system also includes a computer controlled scanning mechanism for updating the position of the film transparency. The algorithm used to determine the velocity vector is discussed in Ref. 5, and its accuracy is estimated at 1% or better.

Typical double exposure photographs of the jet in the central plane through the small dimension of the nozzle, for two different times are shown in Fig. 1. These pictures display the flow field from the nozzle exit to a downstream location of about eight widths. The photographs were taken using the velocity shift and external seeding of the ambient medium. From these and other flow visualization pictures,

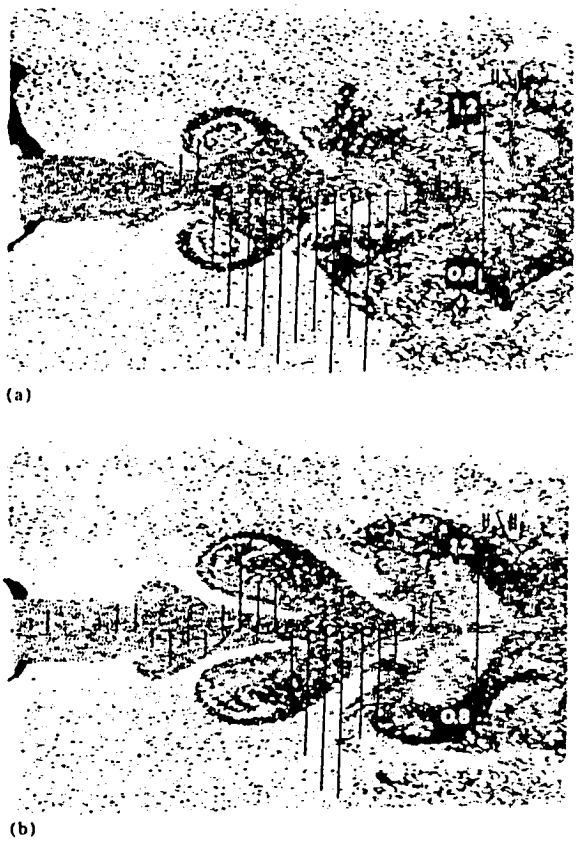

FIG. 1. Instantaneous double exposure photographs of the central plane, containing the small dimension of the jet, and superposed with the jet centerline velocity distribution.

the following observations were made. The jet consists of three regions: the region in which the initial shear layer is unstable and rolls up into discrete vortices; an interaction region in which the vortices pair with each other; and a region in which the vortices break up into random, three-dimensional motion. In spite of the relatively large aspect ratio of the nozzle exit (AR = 4), the rectangular jet organizes itself into a structure similar to that of an axisymmetric jet.[8] The pairing process is also quite similar. In this process, the trailing vortex catches up with the leading vortex, decreases in size, and passes through the leading vortex, which has slowed down and grown in size. The vortex cores rotate around each other and ultimately merge, producing a single vortex. A number of vortex pairings can occur before the vortex becomes three dimensional. The physical regions where these phenomena take place overlap and depend on the phase of the development of the jet. Strong accelerations and decelerations exhibited by the large scale vortical structures can be observed when the instantaneous axial centerline velocity distribution normalized with the jet's axial exit velocity is superimposed on the photographs (Fig. 1). The nondimensional passage frequency of the vortices before pairing is estimated to be about $St_w = 0.7$, where St_w is the Strouhal number based on the nozzle width w and the mean exit velocity U of the jet, i.e., $St_w = fw/U$. This Strouhal number is close to that of an axisymmetric jet,[9] at a comparable Reynolds number. Examination of several photographs

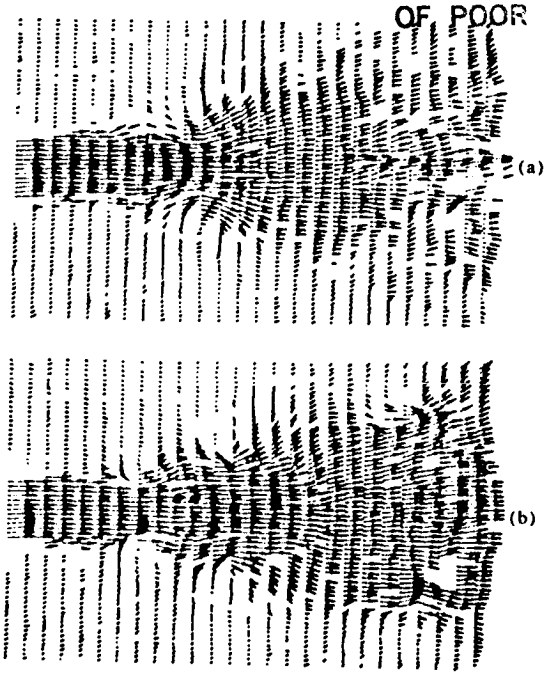

FIG. 2. Instantaneous two-dimensional velocity fields shown in the laboratory reference frame.

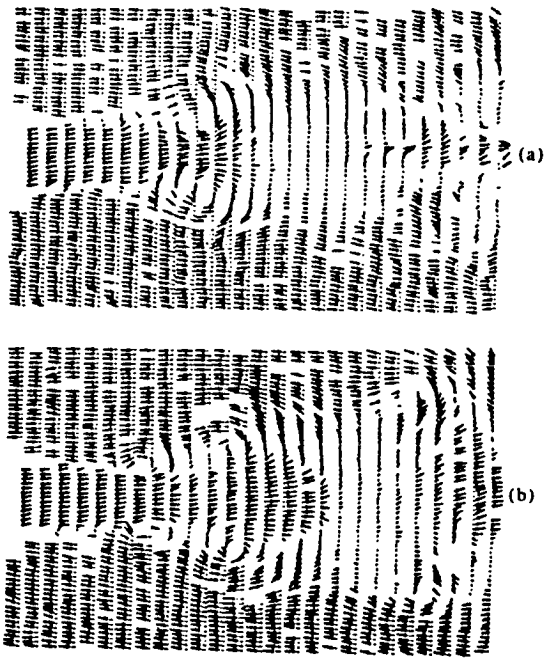

FIG. 3. Instantaneous two-dimensional velocity field shown in a reference frame moving with the convection velocity of the vortical structures.

suggests that the vortex breakdown leads to the larger spreading rate of the jet. The increased three-dimensionality enhances the mixing in the plane of the small dimension of the nozzle. No increase in mixing was observed in the central plane containing the long dimension of the nozzle.

For two typical phases in the development of the jet, shown as the double exposed photographs in Fig. 1, the instantaneous velocity fields were obtained. The results after removal of the velocity bias (i.e., in the laboratory reference frame) are shown as a series of uniformly scaled velocity vectors in Fig. 2. Because the velocity gradients are largest in the transverse direction, the velocity data were acquired using a rectangular mesh with a mesh spacing of 2 mm in the jet axial direction and 0.5 mm in the jet transverse direction. The velocity field displayed in Fig. 2, represents, with great fidelity, all the aforementioned regions of the flow field. These include the shear layers and regions with strongly three-dimensional motion. Such an accurate representation of the flow field was a consequence of our use of the velocity bias technique and the judicious management of the flow seeding procedure.

Examination of the obtained velocity fields confirms our previous analysis based on the flow visualization pictures. The jet structure can be further illuminated when the velocity field is presented in a reference frame moving with the convection velocity of the vortical structure, estimated to be 60% of the jet exit velocity (Fig. 3). In this reference frame, the large scale vortical structures, as well as the nature of the symmetric instability, are clearly observed. The instantaneous velocity profiles provide a unique means to quantify the extent of the jet unsteadiness, the existence of the coherent structures, their interactions, and subsequent generation of random three-dimensional motions.

A successful application of PIDV to study a time dependent, vortical, entraining, and three-dimensional flow field is reported. The data acquired provided quantitative and flow visualization information that revealed the nature of the instability process that occurs in the initial region of the jet. This process is consistent with previously observed features of axisymmetric jets. Furthermore, new and important quantitative information was obtained which is essential for a deeper understanding of this complex flow field.

ACKNOWLEDGMENTS

This work is supported by the Aeromechanics branch of NASA Ames Research Center under Grant No. NAG 2-314. The grant monitor is Dr. C. A. Smith, whose cooperation and understanding is much appreciated.

[1] R. Meynart, Phys. Fluids **26**, 2074 (1983).
[2] C. C. Landreth, R. J. Adrian, and C. S. Yao, Exp. Fluids **6**, 119 (1988).
[3] A. Krothapalli, D. Baganoff, and K. Karamcheti, J. Fluid Mech. **107**, 201 (1981).
[4] C. M. Ho and E. Gutmark, J. Fluid Mech. **179**, 383 (1987).
[5] L. M. Lourenco and A. Krothapalli, Exp. Fluids **5**, 29 (1987).
[6] L. M. Lourenco and A. Krothapalli, *Laser Anemometry in Fluid Mechanics-III* (Ladon-Institute Superior Technico, Lisbon, Portugal, 1988), p. 161.
[7] L. M. Lourenco, A. Krothapalli, J. M. Buchlin, and M. L. Riethmuller, in *Aerodynamic and Related Hydrodynamic Studies Using Water Facilities*, AGARD CP-413 (NATO, Brussels, 1986), paper 23.
[8] E. E. Bouchard, Ph.D. dissertation, Stanford University, 1982.
[9] H. A. Becker and T. A. Massaro, J. Fluid Mech. **31**, 435 (1968).